Supplementary

Solvent tuned discriminant sensing of Al^{3+}, Mg^{2+} and HF_2^- by vanilinyl-picolinyl hydrazide Schiff base

Rakesh Purkait, Chittaranjan Sinha*

Department of Chemistry, Jadavpur University, Kolkata 700 032, India, crsjuchem@gmail.com

Experimental Section

Materials and methods

All the required inorganic salts and organic chemicals of AR quality were obtained from Sigma-Aldrich and Merck, and used without further purification. Aqueous solutions of the required salts were prepared using Milli-Q water (Millipore). Perkin-Elmer 2400 Series-II CHN analyzer, Perkin Elmer, USA elemental analyser was used for elemental analyses. UV-vis spectra were taken from Perkin Elmer Lambda 25 spectrophotometer and fluorescence spectra were obtained by using a Perkin Elmer spectrofluorimeter model LS55; Fluorescence lifetime measurements were carried out by using time-correlated single photon counting set up from Horiba Jobin-Yvon; FT-IR spectra (KBr disk, 4000–400 cm^{-1}) were collected from a Perkin Elmer LX-1 FTIR spectrophotometer. ^1H NMR spectra were obtained on a Bruker (AC) 300 MHz FT-NMR spectrometer and TMS is used as an internal standard. ESI mass spectra were recorded from a Water HRMS model XEVO-G2QTOF#YCA351 spectrometer. All of the required experimental measurements were conducted at room temperature.

Synthesis of HVPh

Picolino hydrazide was prepared from Picolinic acid. With continuous stirring to the MeOH (7 ml) solution of Picolino hydrazide (137.13 mg, 1.0 mmol), 2-hydroxy-4-methoxy-benzaldehyde (152.14 mg, 1.0 mmol) in methanol solution (7 ml) was added drop-by-drop

and stirring was continued for 8 h. Then the resultant clear solution was kept and allowed for slow evaporation, crystalline product was obtained after two weeks in 94% yield. Pyridine-2-carboxylic acid (2-hydroxy-4-methoxy-benzylidene)-hydrazide (**HVPh**) : M.P.>200 °C. The mass spectrum displays an ion peak at 272.1420 for [**HVPh**+H]$^+$ and a base peak at 294.1283 which corresponds the formation of [**HVPh** +Na]$^+$ (**Fig. S1**); Microanalytical data: $C_{14}H_{13}N_3O_3$ calcd (found): C, 61.99 (61.81); H, 4.83 (4.90); N, 15.49 (14.58); %. ^{1}H NMR (300 MHz, DMSO-d_6): δ12.39 (s, 1H, NH), 11.74 (s, 1H, OH), 8.74 (s, 1H, imine-H), 8.72 (d, 1H, Pyridine), 8.14-8.03 (m, 2H, pyridine), 7.69-7.65 (m, 1H, pyridine),7.34 (d, 1H, vaniline), 6.54 (d. 1H, vaniline), 6.50 (t, 1H, vaniline), 3.78 (s, 1H, OCH_3) (**Fig. S2**); IR: 3461 cm^{-1} (phenolic-OH), 3467 cm^{-1} (hydrazide -NH), 1664 cm^{-1} (imines C=N). (**Fig. S3**).

UV–Vis and fluorescence spectral studies

The stock solution of **HVPh** (1×10^{-3} mol L^{-1}) was prepared in DMSO. For the fluorescence and UV-Visible spectral study, the solution of **HVPh** was diluted to 20×10^{-6} mol L^{-1} with DMSO and Water. For UV-vis and fluorescence experiments, the test samples were prepared by placing appropriate amounts of the stock solution of the respective cations into 2.0 mL of the probe solution. For fluorescence measurements, the excitation was provided at 340 nm, and emission was acquired from 370 nm to 660 nm (excitation slit = 15.0 and emission slit = 5.0). Spectral data were taken within 10 seconds after addition of the ions.

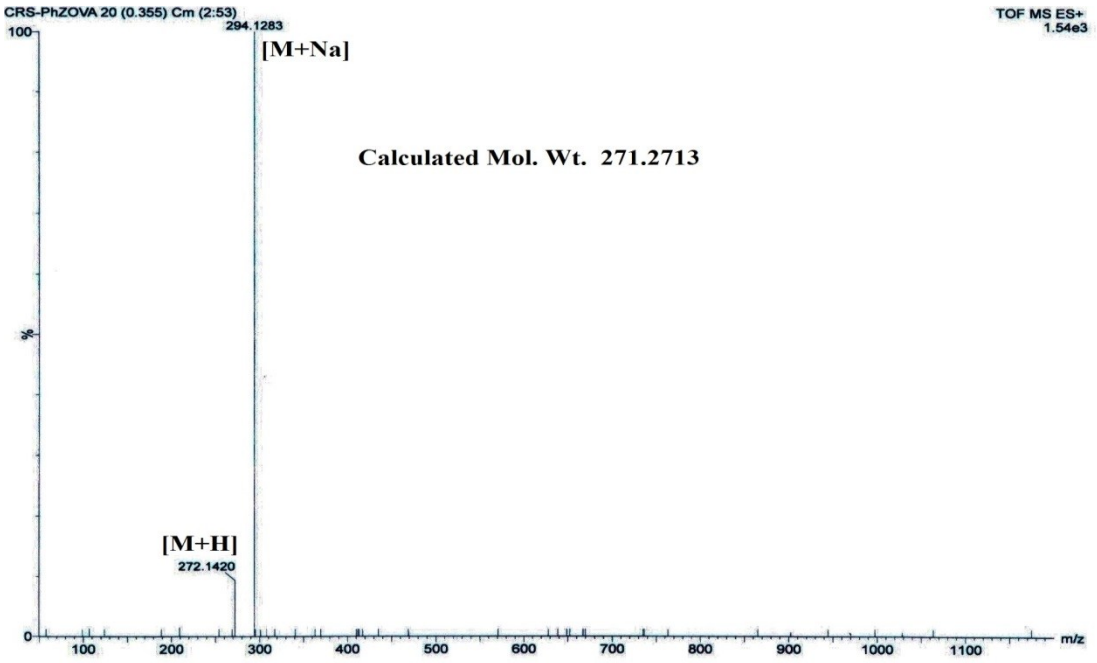

Fig S1 Mass spectrum of **HVPh**

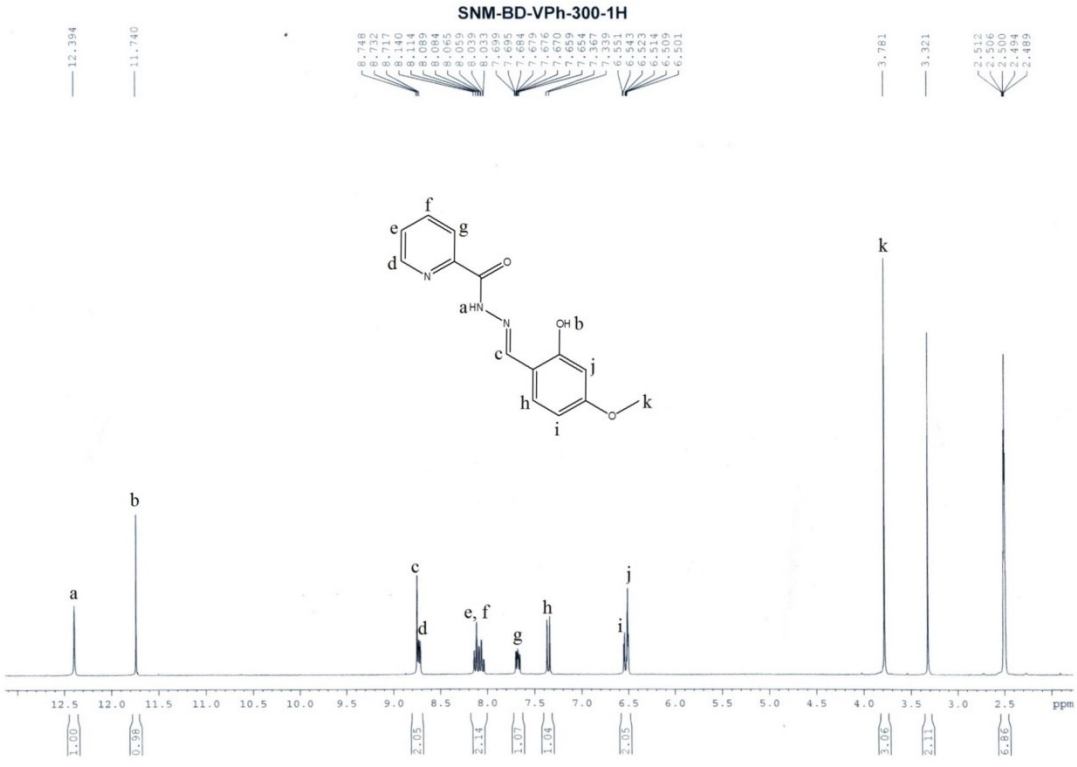

Fig S2 ^{1}H NMR of **HVPh** in DMSO-d_6

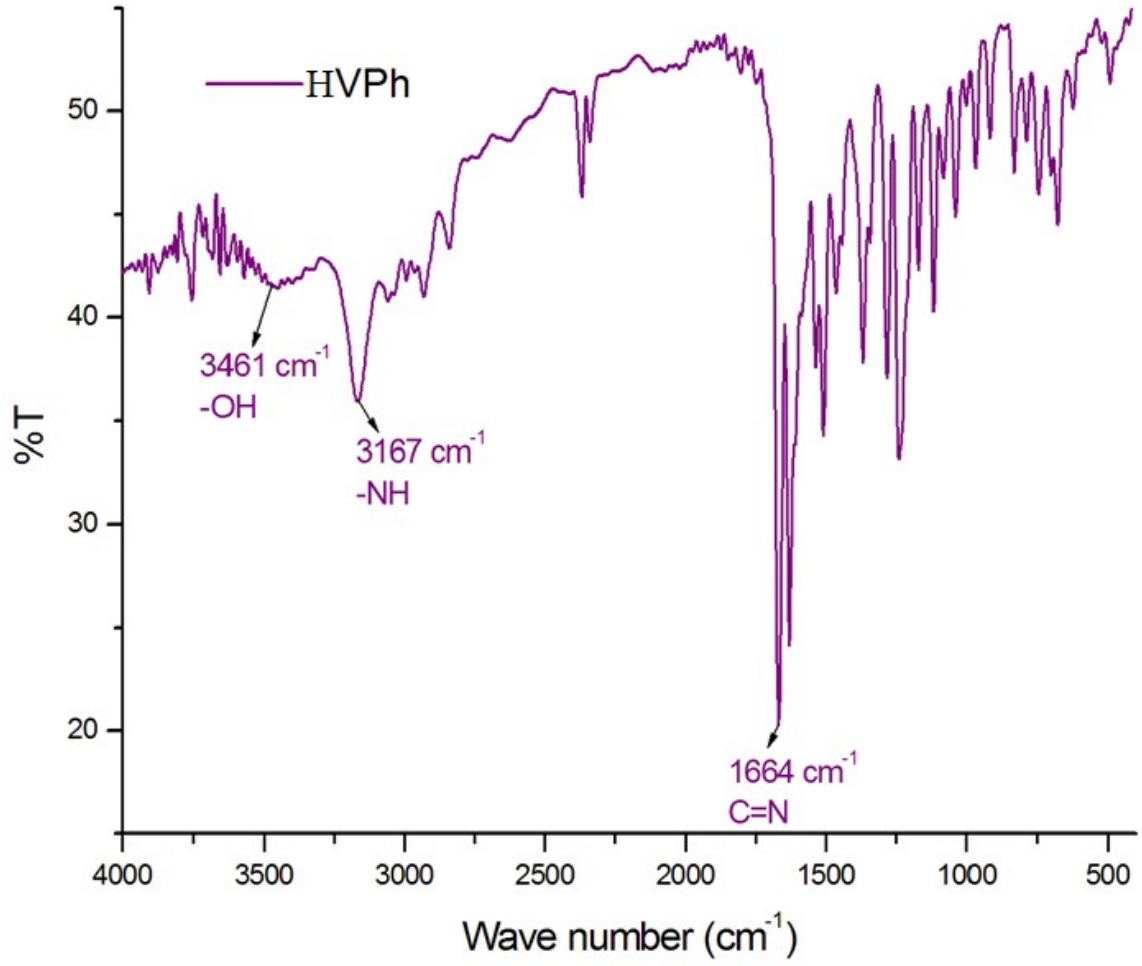

Fig S3 IR spectrum of **HVPh** in KBr disk.

Table S1 Single Crystal X-ray diffraction data of **HVPh**

Empirical formula	$C_{14}H_{13}N_3O_3$
Formula weight	271.27
Temperature (K)	296(2)
System	triclinic
Space group	P -1
a (Å)	13.956(9)
b (Å)	15.246(7)

c (Å)	15.246(7)
α/°	77.91
β/°	62.76
γ/°	62.76
V $(Å)^3$	2564(2)
Z	8
Dc/g cm^{-3}	1.406
μ/mm^{-1}	0.102
θ range/°	1.502– 24.998
F(000)	1136.0
Refine parameters	730
Total reflections	7516
R_1[a][I>2σ(I)]	0.1076
wR_2[b]	0.3265
GOF[c]	0.915

[a]$R_1 = \Sigma||F_o|-|F_c||/\Sigma|F_o|$; [b]$wR_2 = \{\Sigma[w(F_o^2-F_c^2)^2]/\Sigma[w(F^2_o)^2]\}^{1/2}$; $w = [\sigma^2(F_o)^2 + (0.1003P)^2 + 4.9693P]^{-1}$ $(F_o^2 + 2F_c^2)/3$; [c] Goodness-of-fit

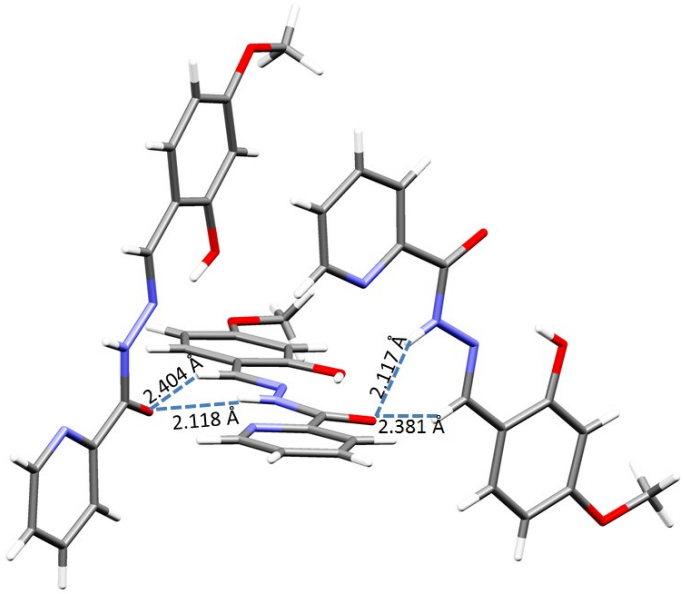

Fig S4 Inter-molecular H-bonding in **HVPh**

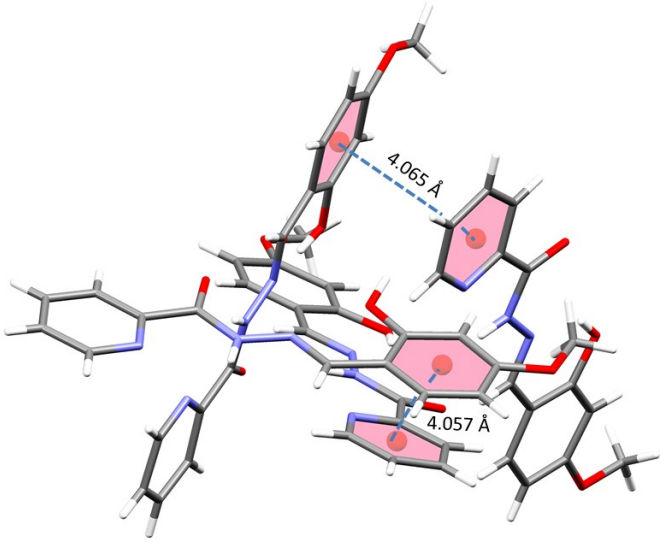

Fig S5 Inter-molecular π… π stacking in **HVPh**

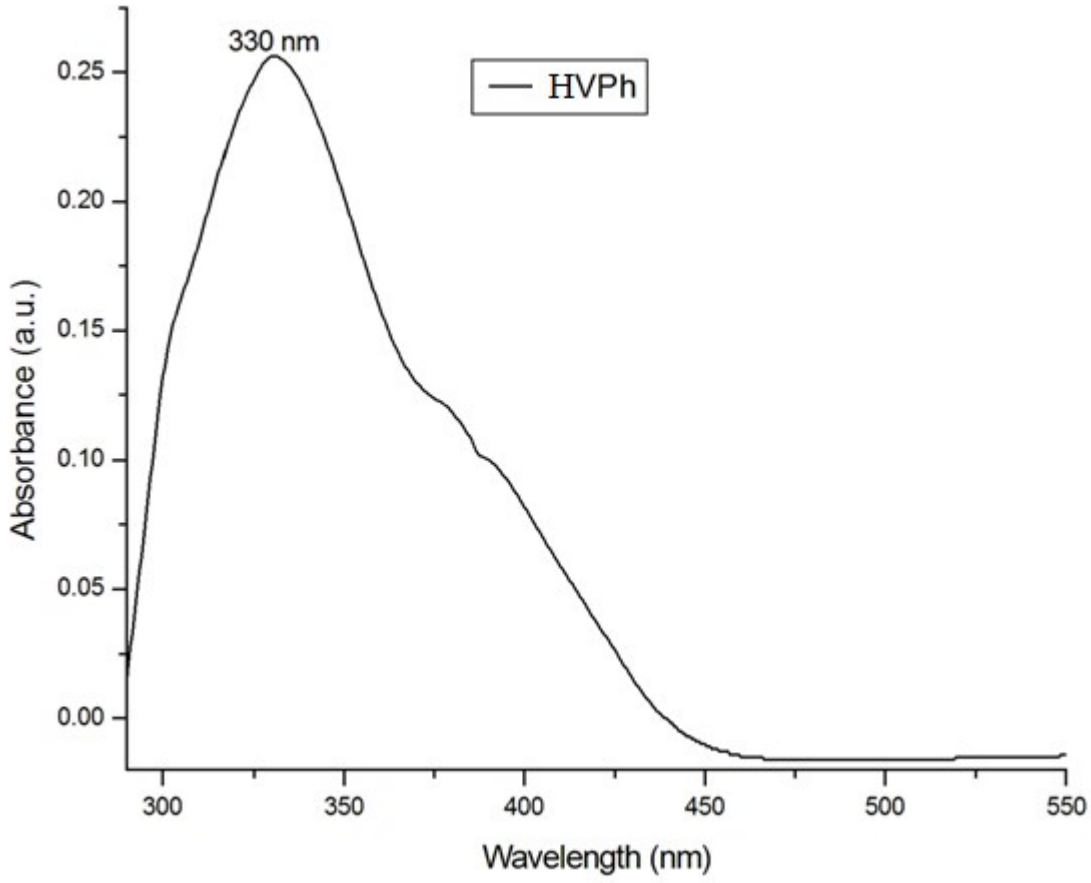

Fig S6 UV-vis spectrum of **HVPh** in Water medium.

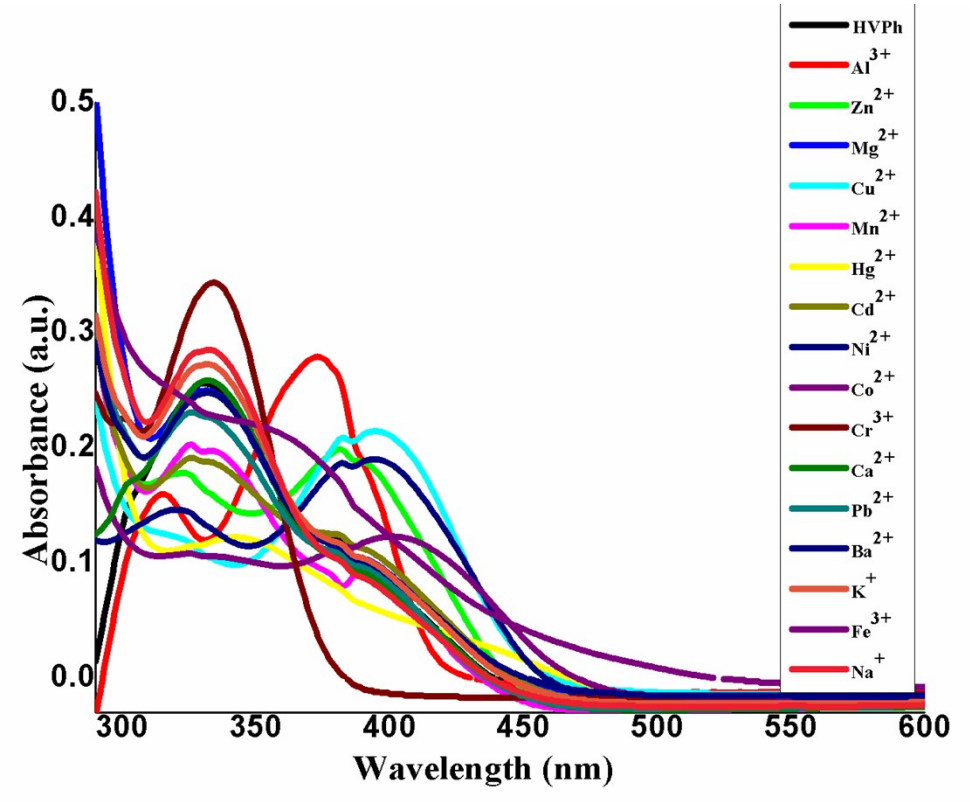

Fig S7 UV-vis spectra of **HVPh** upon addition of various metal ions in water medium.

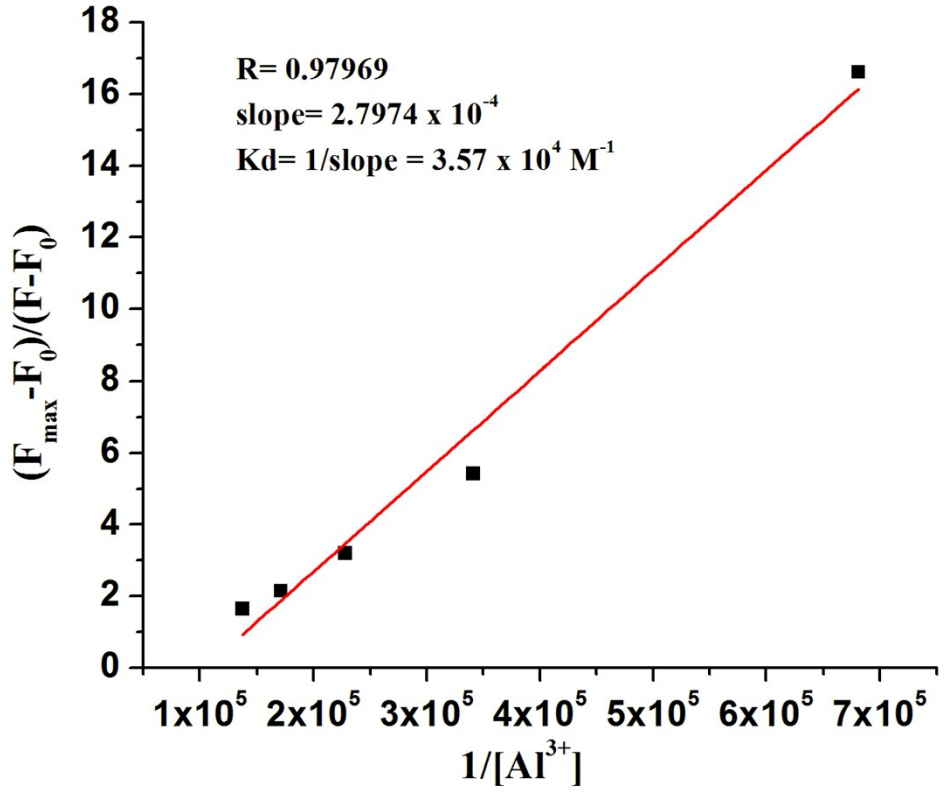

(**a**)

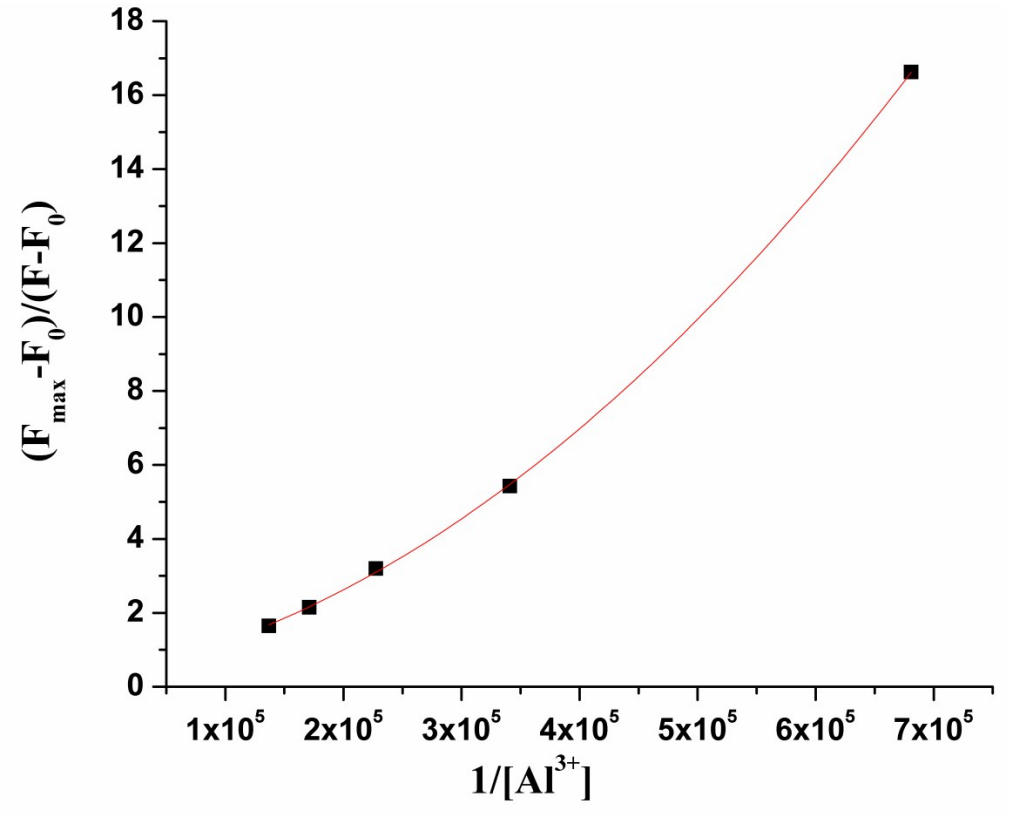

(b)

Fig S8 Fluorescence titration determine binding constant using Benisi-Hildebrand method for Al^{3+} [(a) Linear fitting; (b) Non-linear fitting]

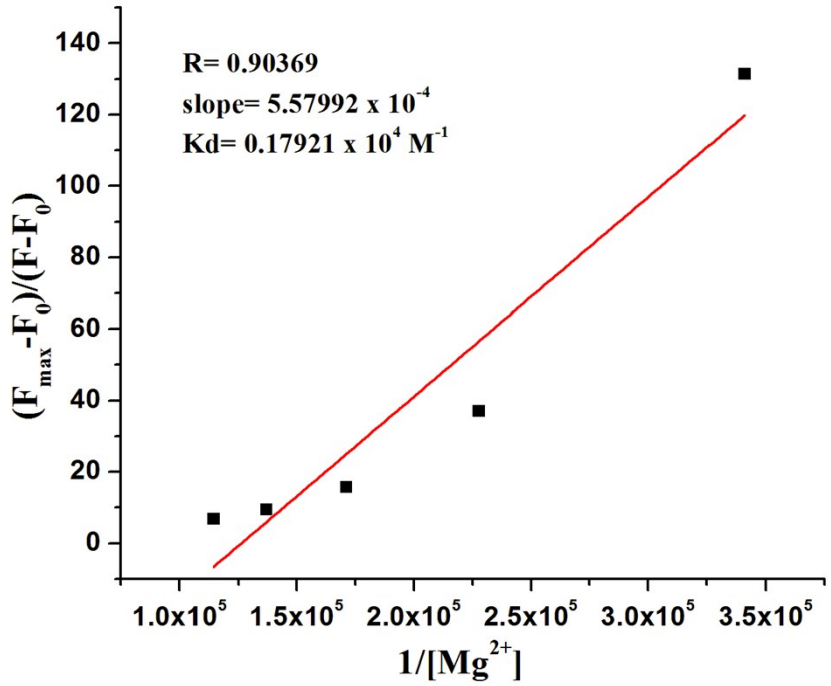
R= 0.90369
slope= 5.57992 x 10^-4
Kd= 0.17921 x 10^4 M^-1
(F_max-F_0)/(F-F_0)
1/[Mg^2+]
0
20
40
60
80
100
120
140
1.0x10^5
1.5x10^5
2.0x10^5
2.5x10^5
3.0x10^5
3.5x10^5

(a)

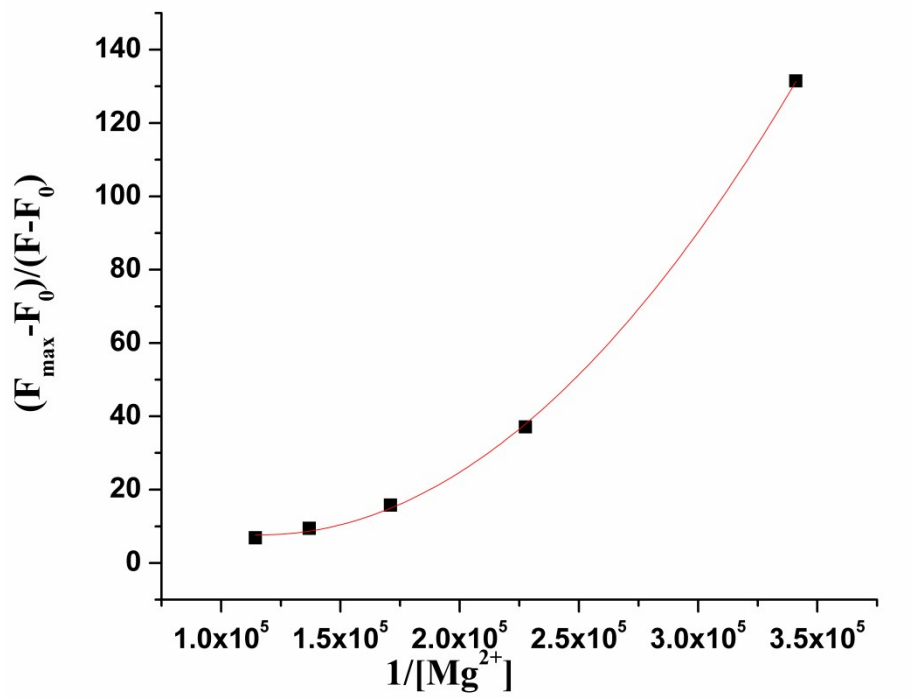
(F_max-F_0)/(F-F_0)
1/[Mg^2+]
0
20
40
60
80
100
120
140
1.0x10^5
1.5x10^5
2.0x10^5
2.5x10^5
3.0x10^5
3.5x10^5

(**b**)

Fig S9 Fluorescence titration determines binding constant using Benisi-Hildebrand method for Mg^{2+} [(a) Linear fitting; (b) Non-linear fitting]

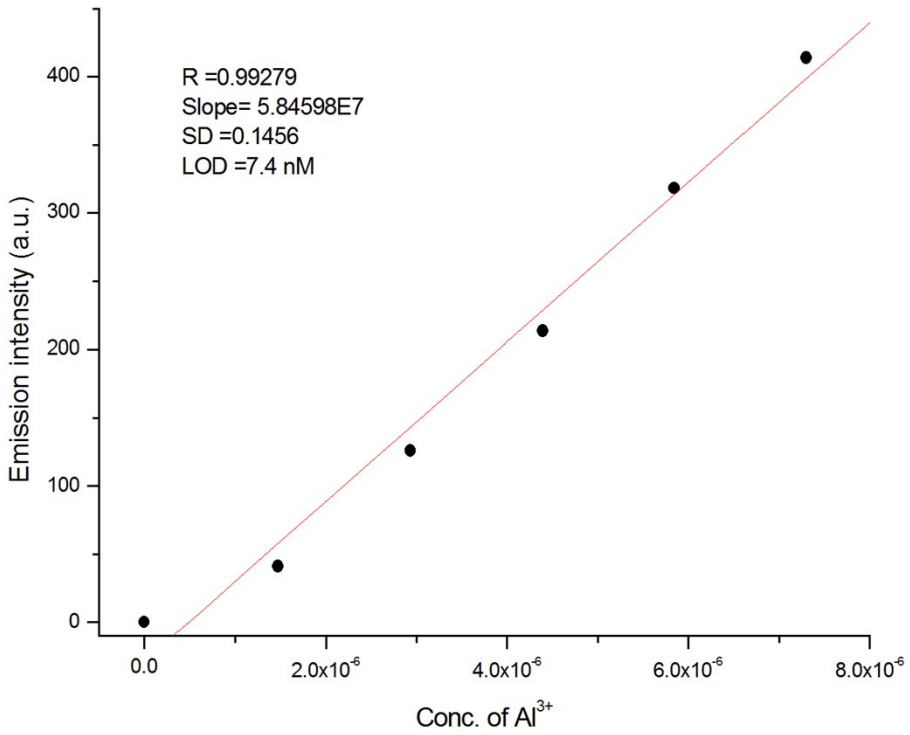

Fig S10 Calculation of limit of detection (LOD) for Al^{3+}

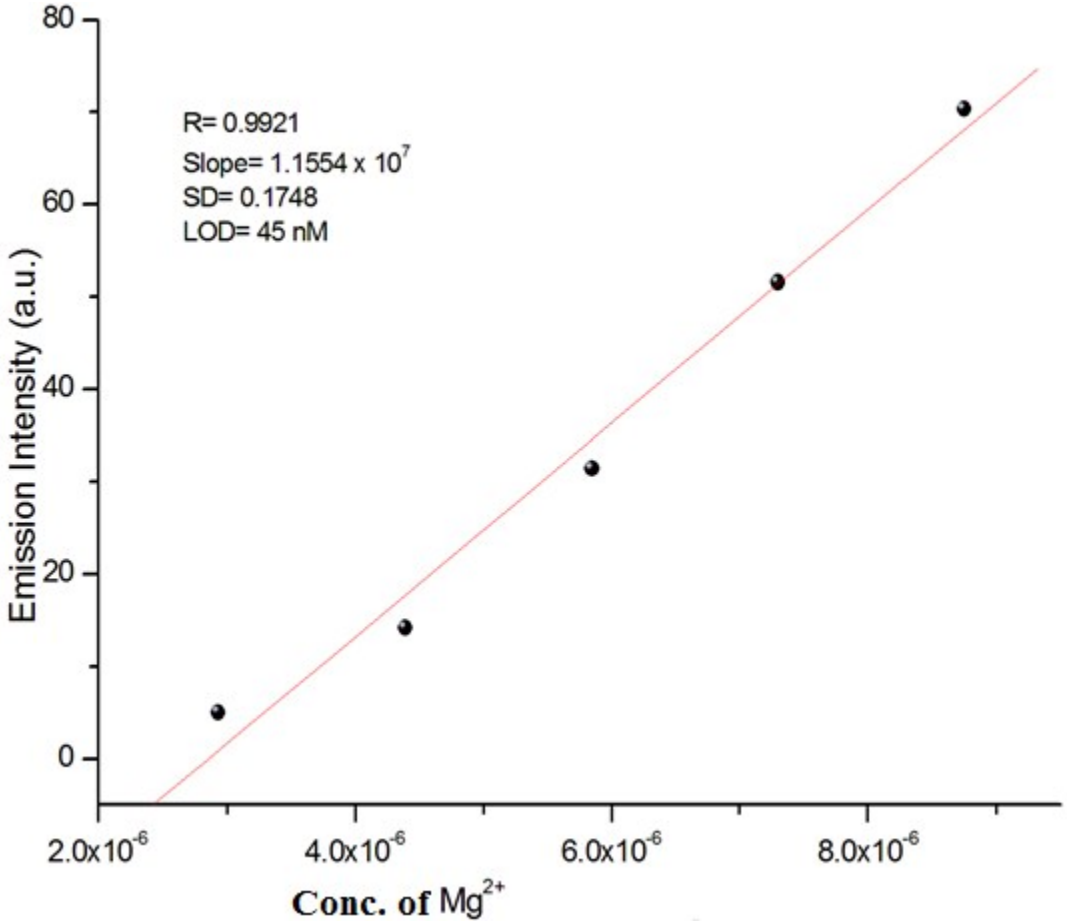

Fig S11 Calculation of limit of detection (LOD) for Mg^{2+}

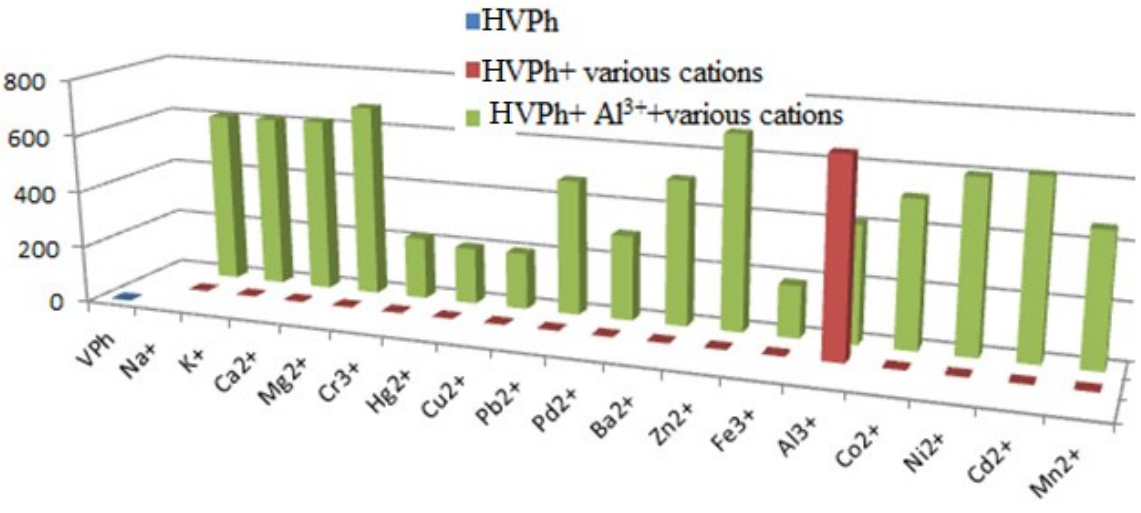

Fig S12 Studies of interference by various metal ions on Al^{3+} sensitivity

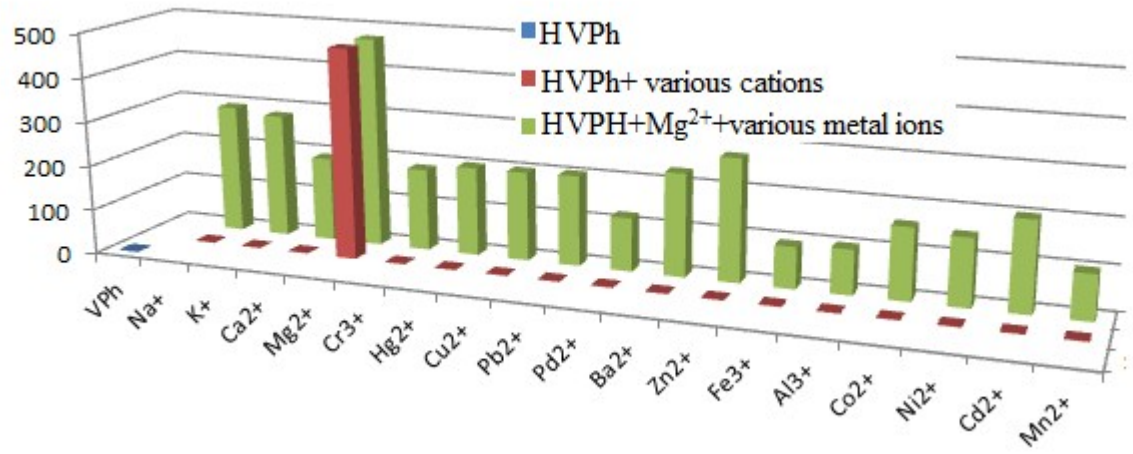

Fig S13 Studies of interference by various metal ions on Mg^{2+} sensitivity

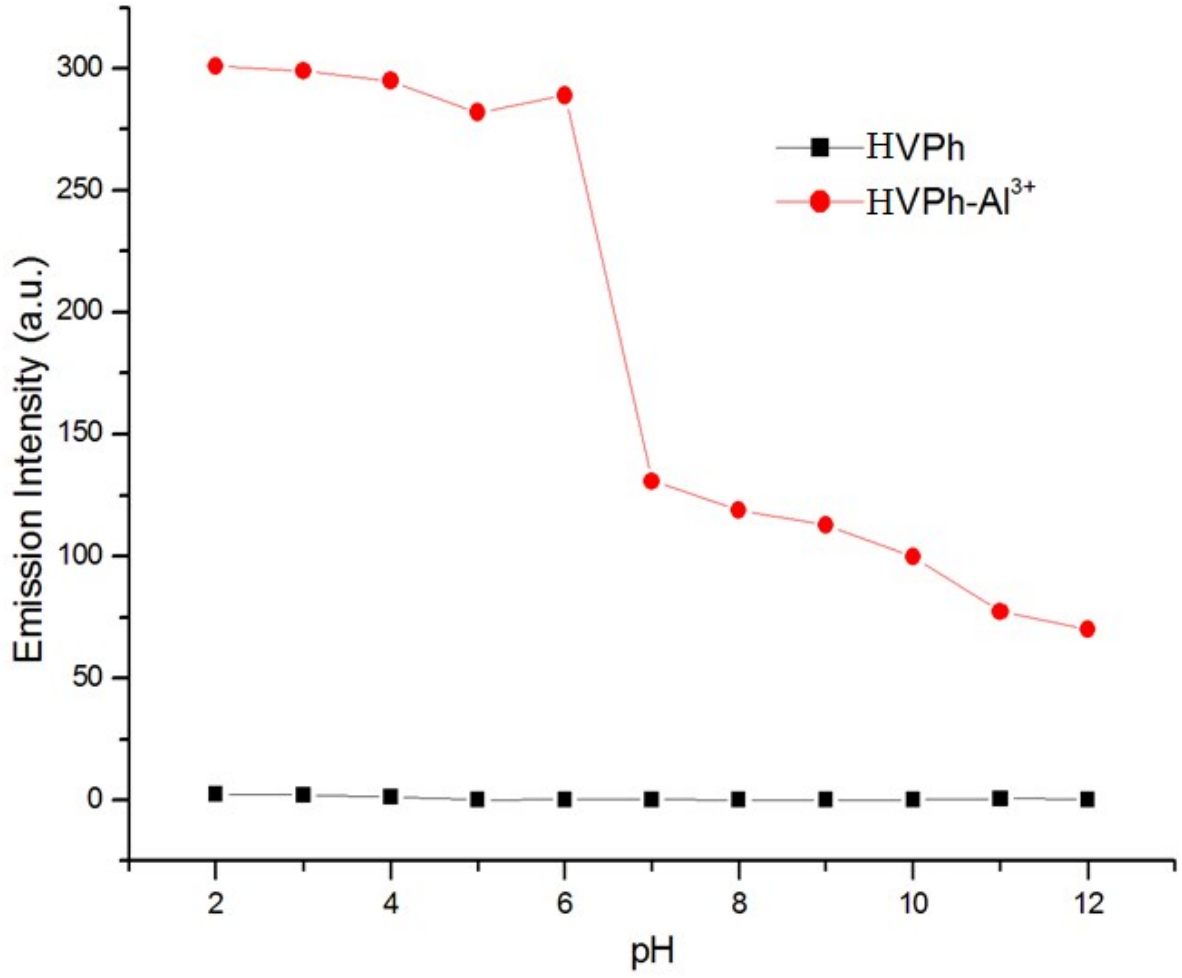

Fig S14 pH variation sensitivity of **HVPh** towards Al^{3+}

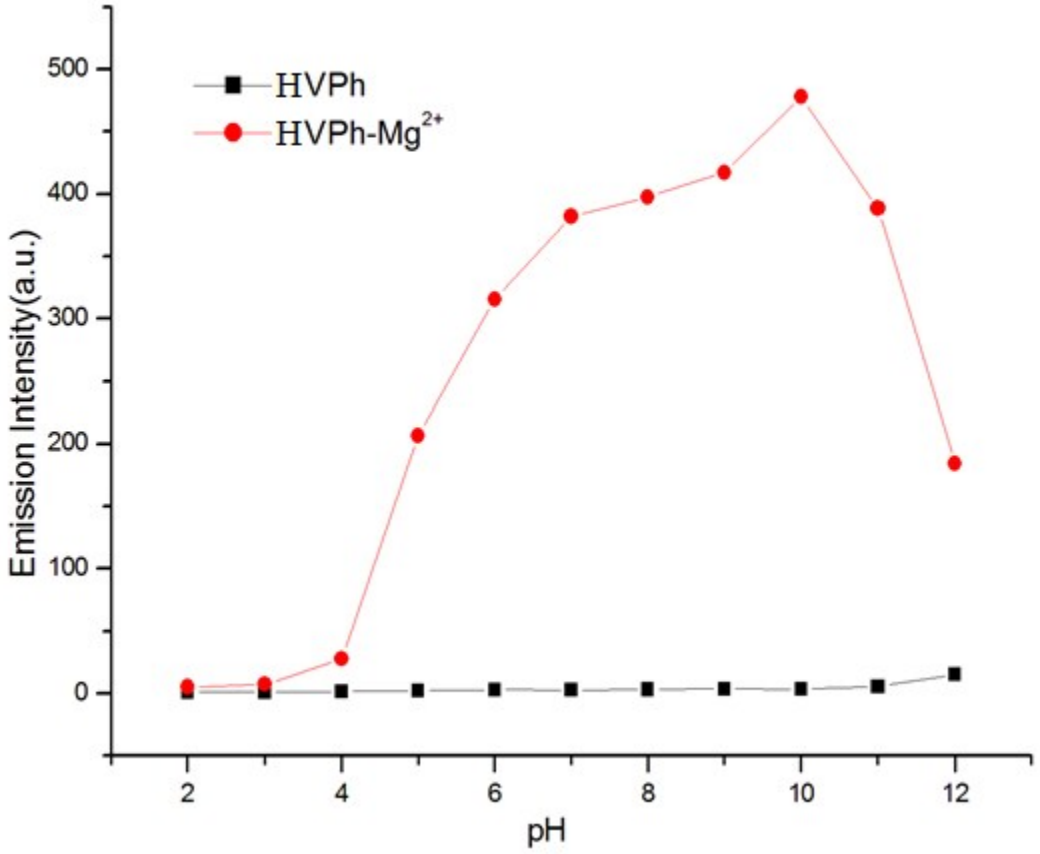

Fig S15 pH variation sensitivity of **HVPh** towards Mg^{2+}

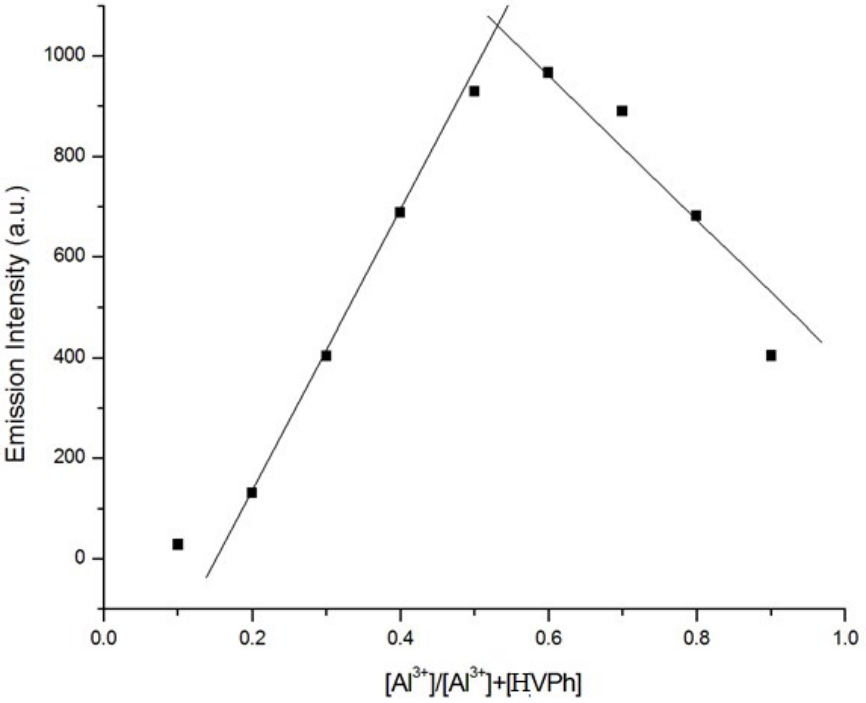

Fig S16 Job's plot for Al^{3+} by fluorescence spectroscopy

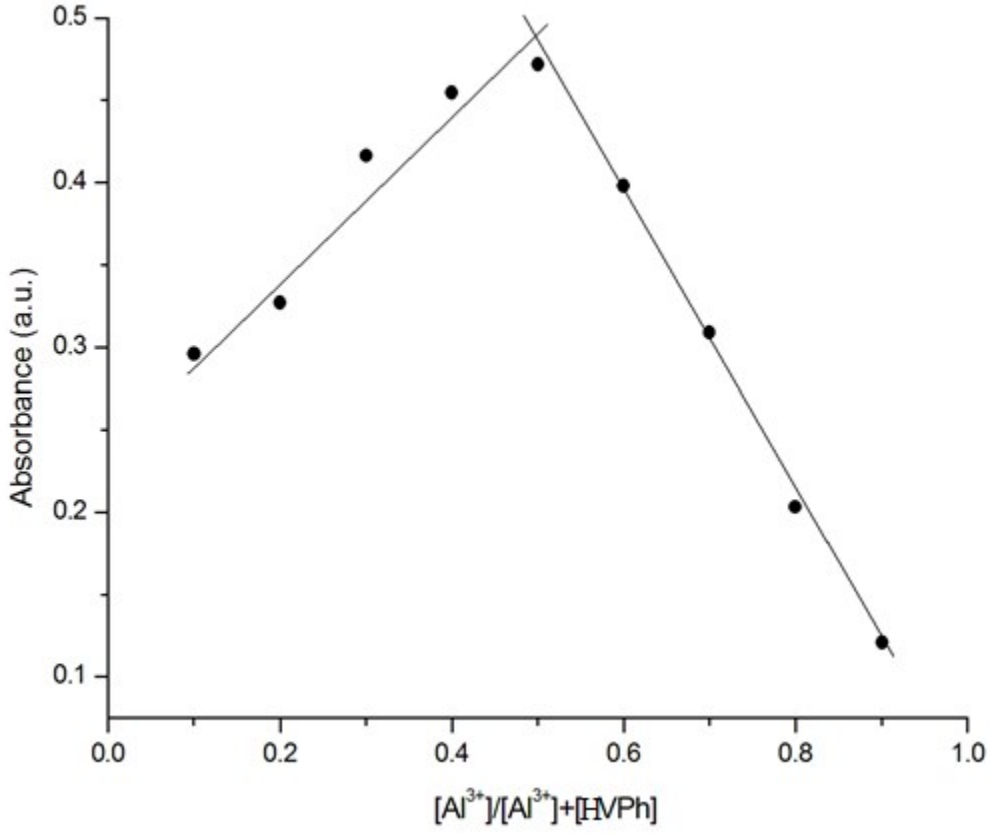

Fig S17 Job's plot for Al^{3+} by UV-vis spectroscopy

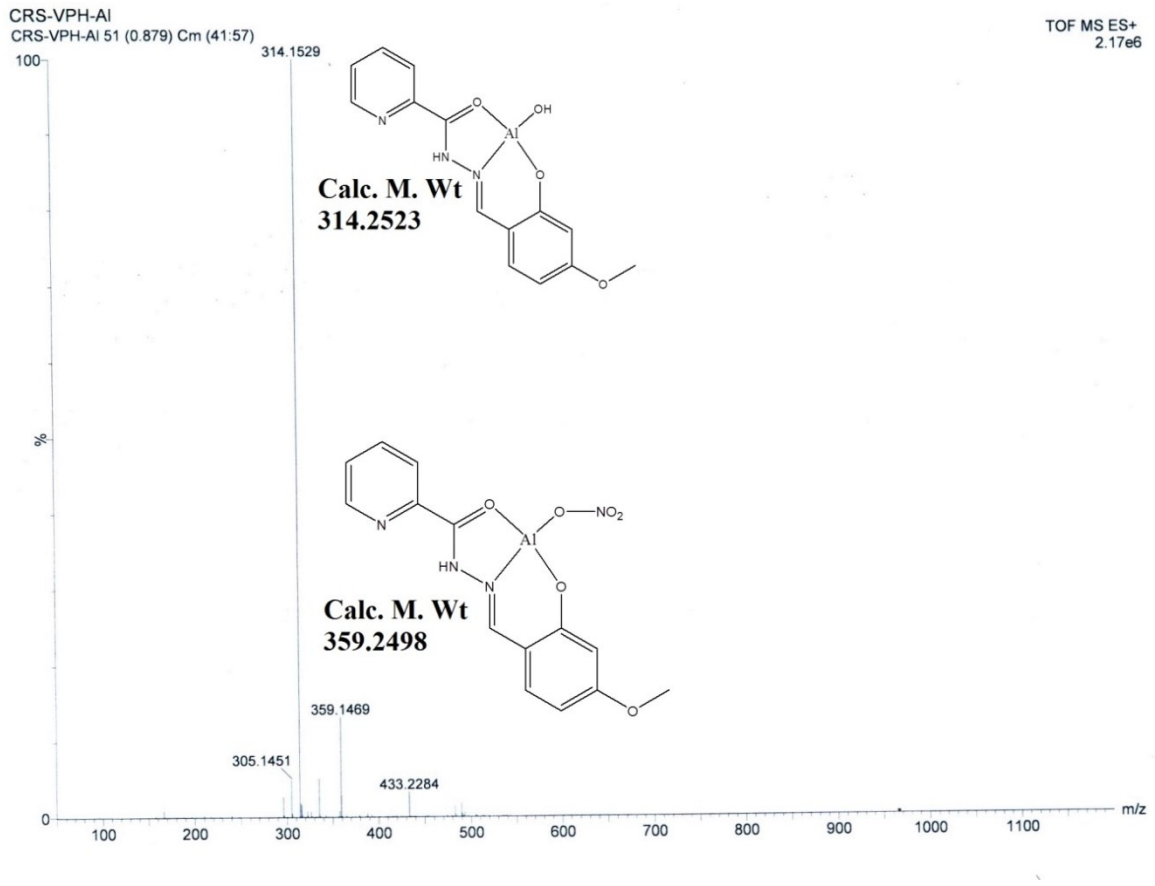

Fig S18 Mass spectra of **HVPh**-Al complex

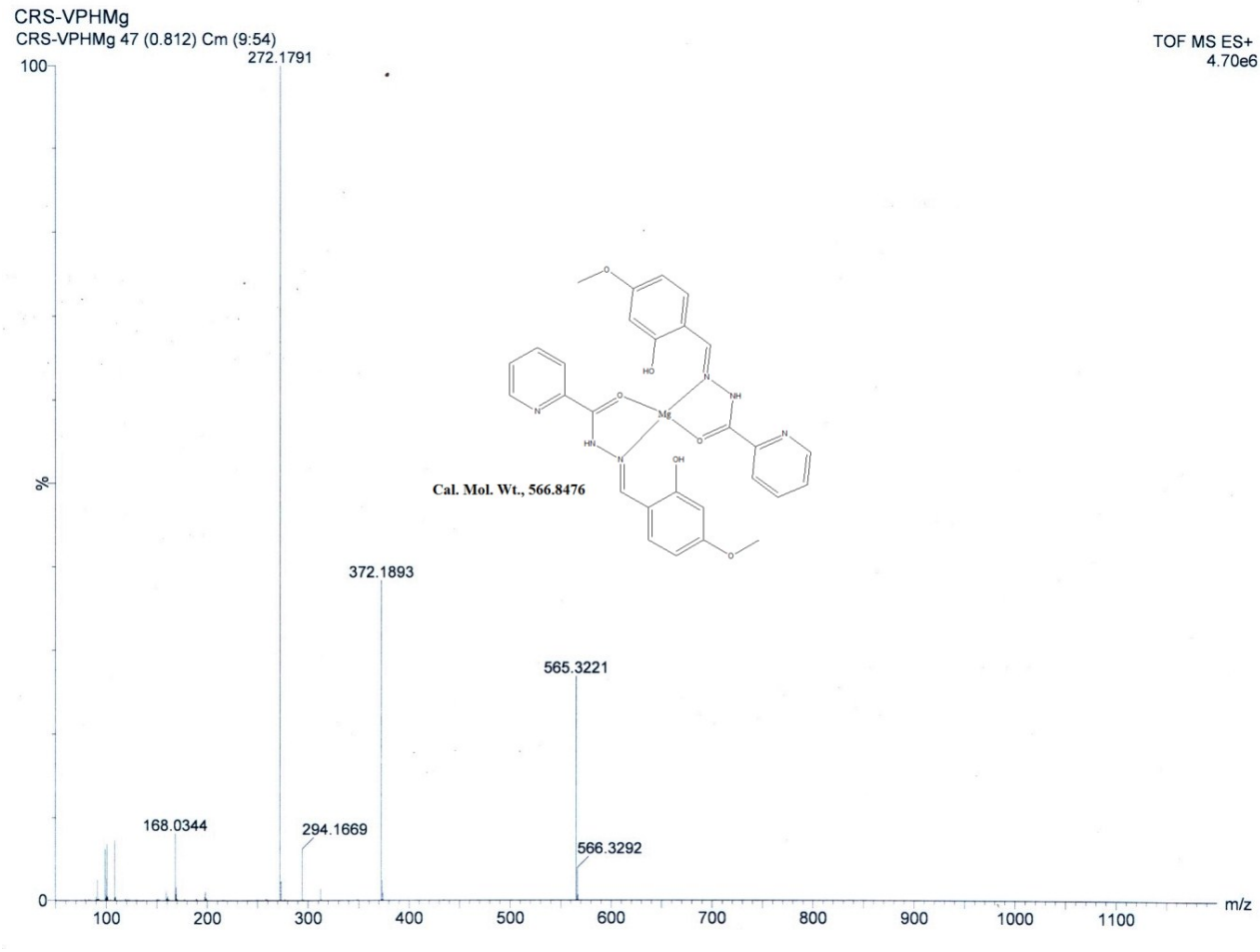

Fig S19 Mass spectra of **HVPh**-Mg complex

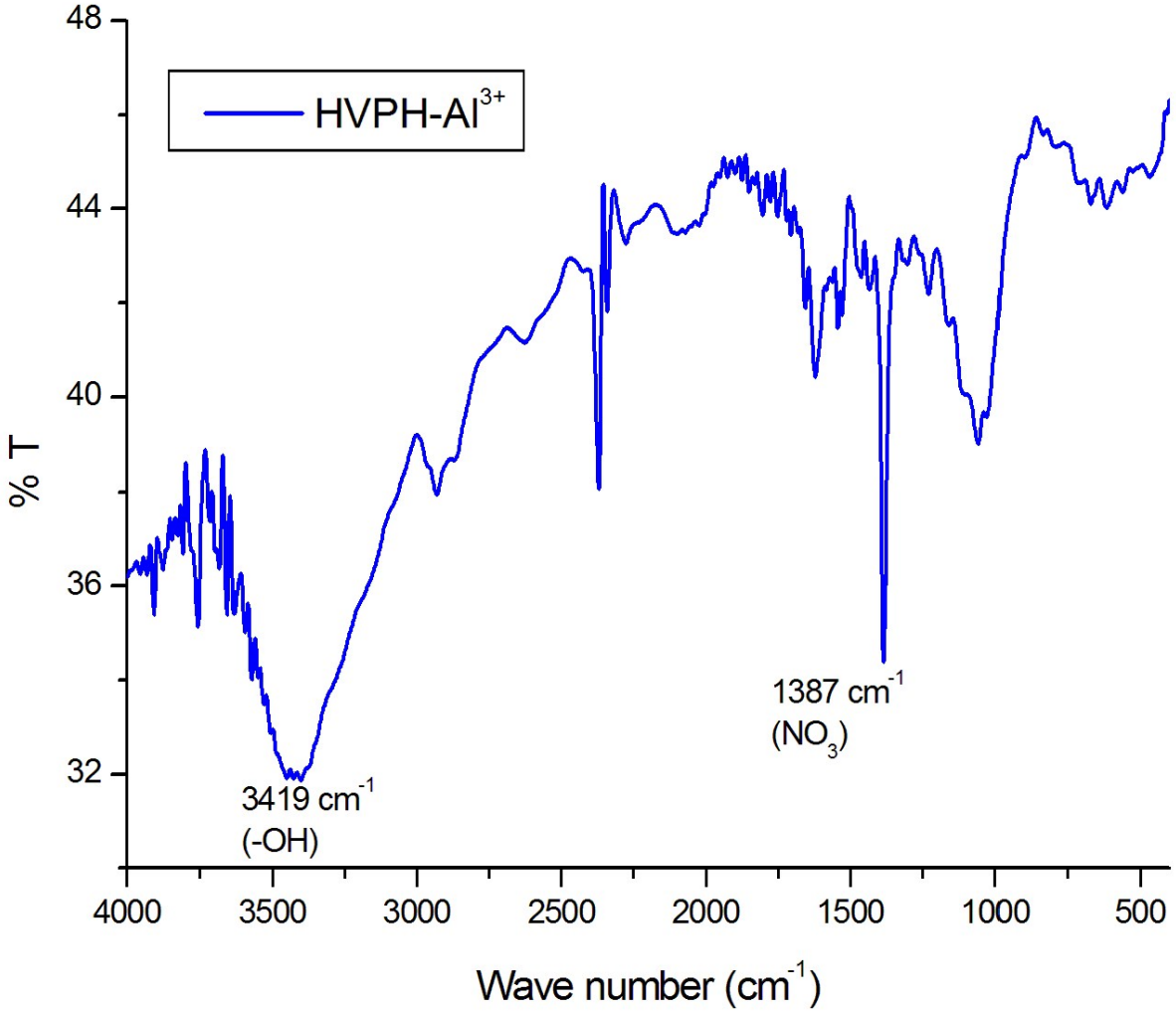

Fig S20 IR spectrum of **HVPh**-Al complex in KBr disk

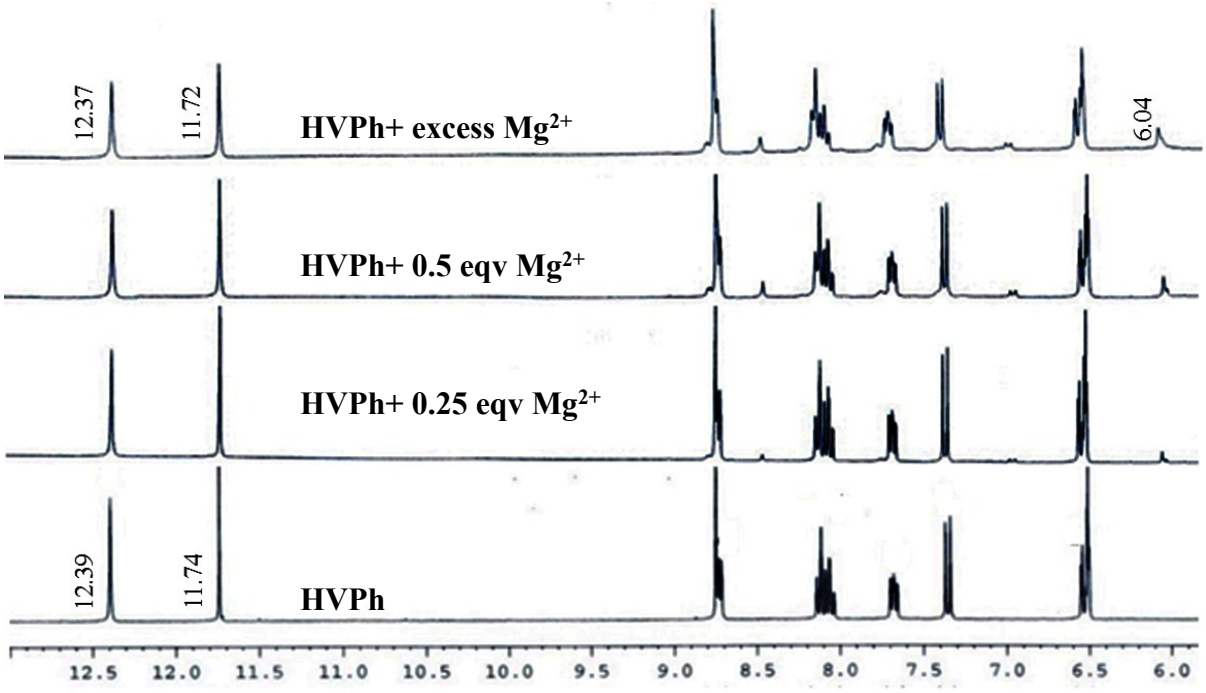

Fig S21 ^{1}H NMR spectra of **HVPh** in DMSO-d_6 on gradual addition of Mg^{2+} salt.

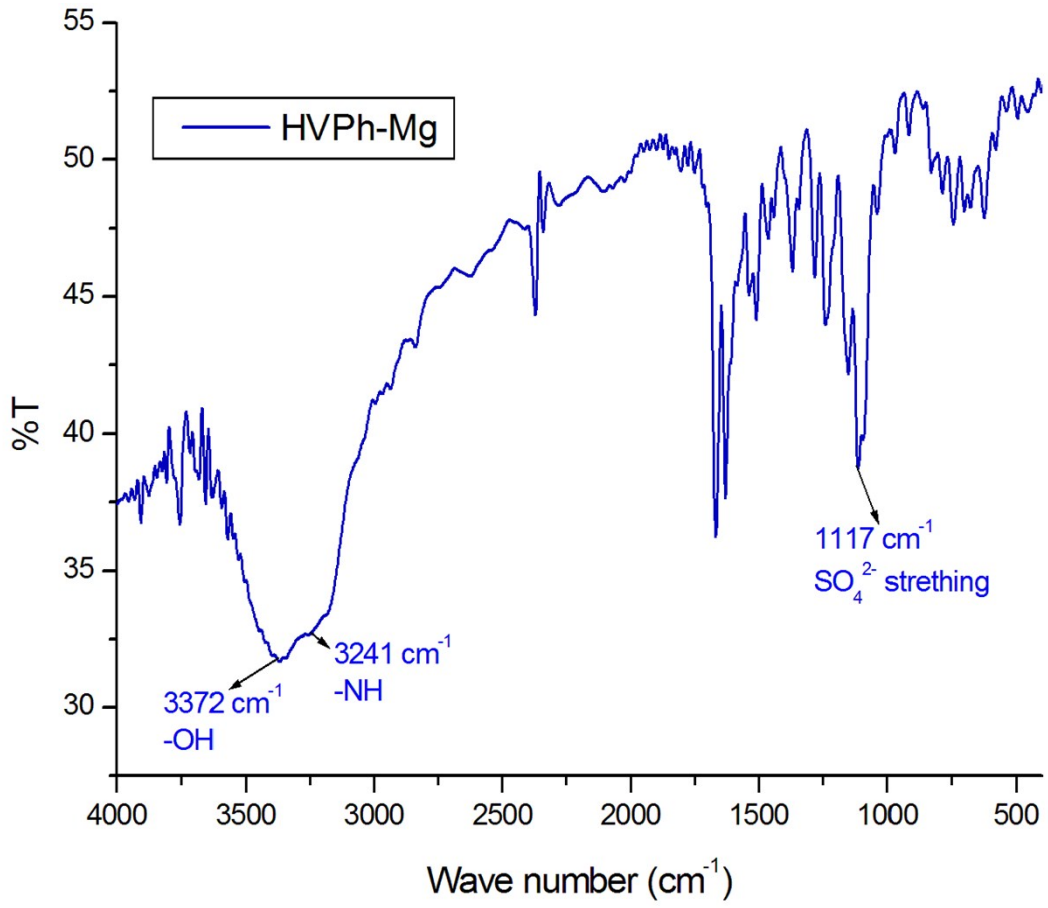

Fig S22 IR spectrum of **HVPh**-Mg in KBr disk

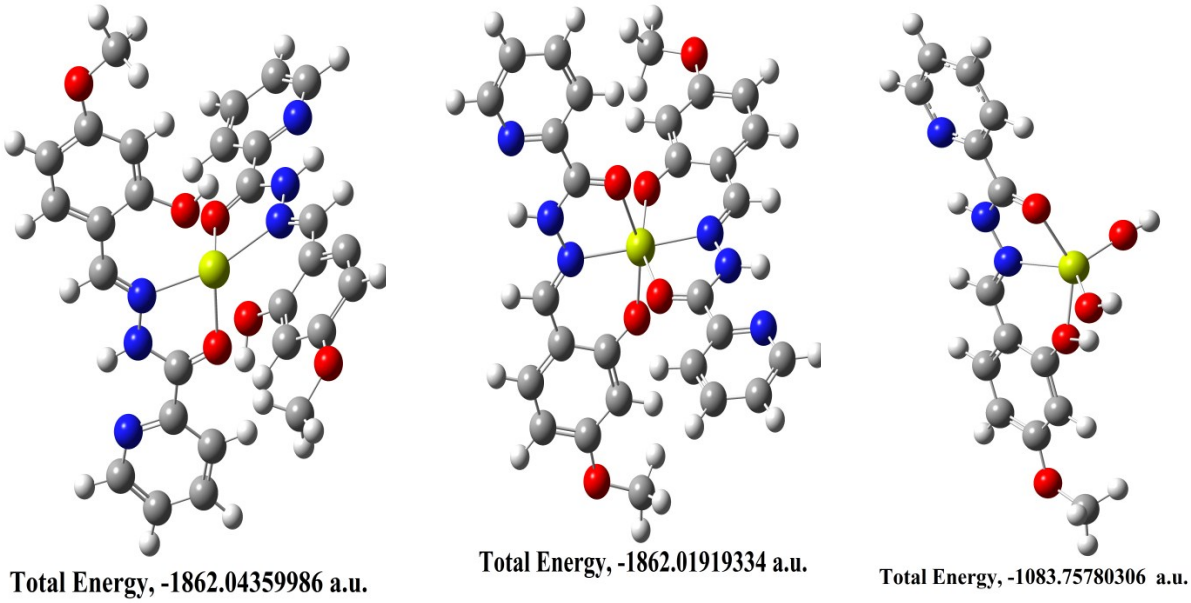

(A) (B) (C)

Fig S23 DFT optimised structure with total energy of probable Mg^{2+} complex of **HVPh** (A) charged (+2); (B) Neutral; (C) Mg^{2+} Complex as **HVPh**-Al.

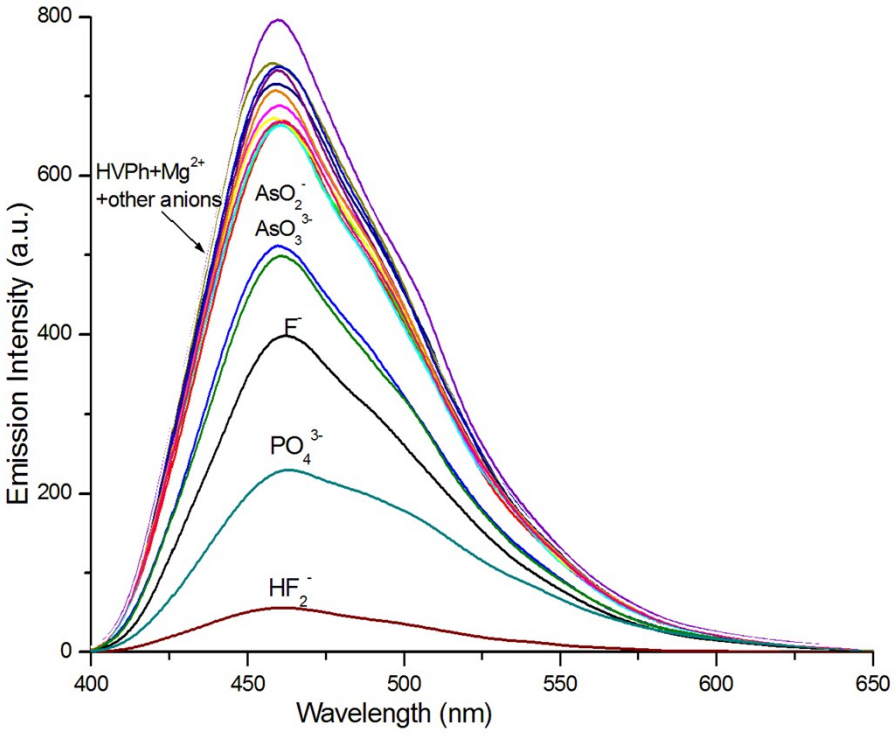

Fig S24 Interaction of **HVPh**-Al^{3+} with various anions in Fluorescence spectroscopy

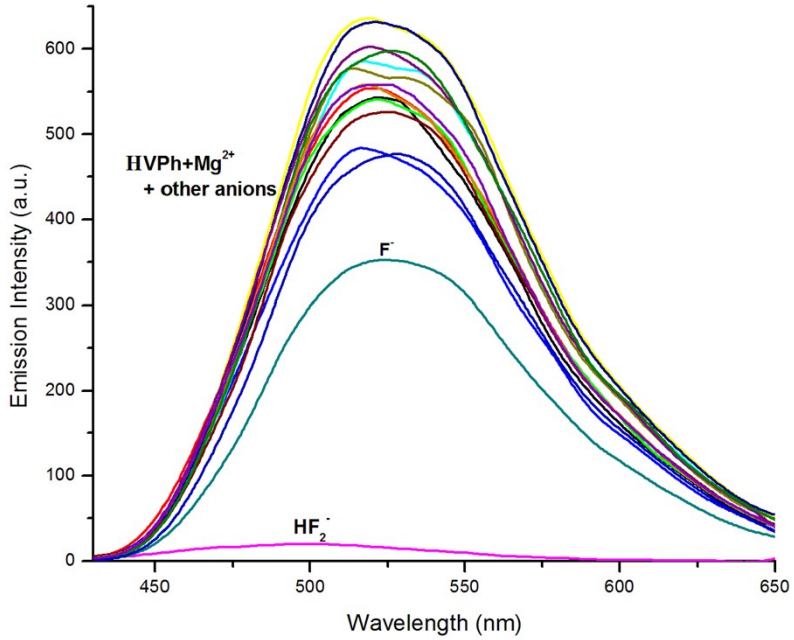

Fig S25 Interaction of **HVPh**-Mg^{2+} with various anions in Fluorescence spectroscopy. Anions are $S_2O_3^{2-}$ ($Na_2S_2O_3$, $5H_2O$), SCN^-(NH_4SCN), PO_4^{3-}(K_3PO_4, H_2O), OAc^- (NaOAc, $3H_2O$), ClO_4^-($NaClO_4$), SO_4^{2-}(Na_2SO_4), HSO_4^-($NaHSO_4$), Cl^- (NaCl), F^-(NaF), HF_2^- (NH_4HF_2), NO_3^-(KNO_3), Br^- (KBr), NO_2^-($NaNO_2$), N_3^-(NaN_3), AsO_4^{3-}(Na_3AsO_4), AsO_2^- ($NaAsO_2$).

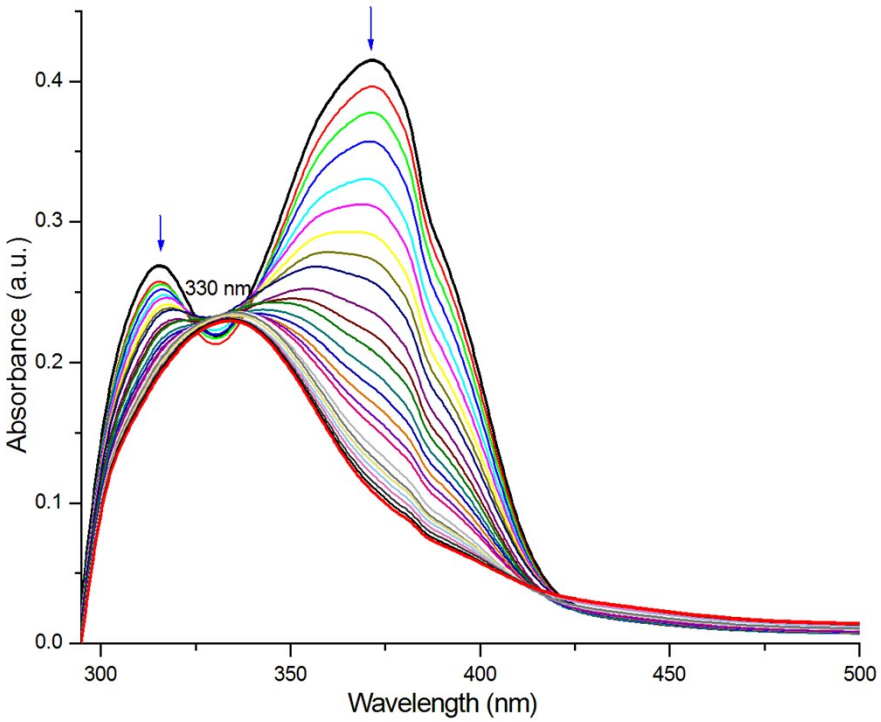

Fig. S26. Changes observed on incremental addition of HF_2^- (0.003 ml × 10^{-3} M each) to in situ formed 1:1 **HVPh**-Al^{3+} in H_2O (pH 7.2, HEPES buffer) in (14) UV-vis spectra.

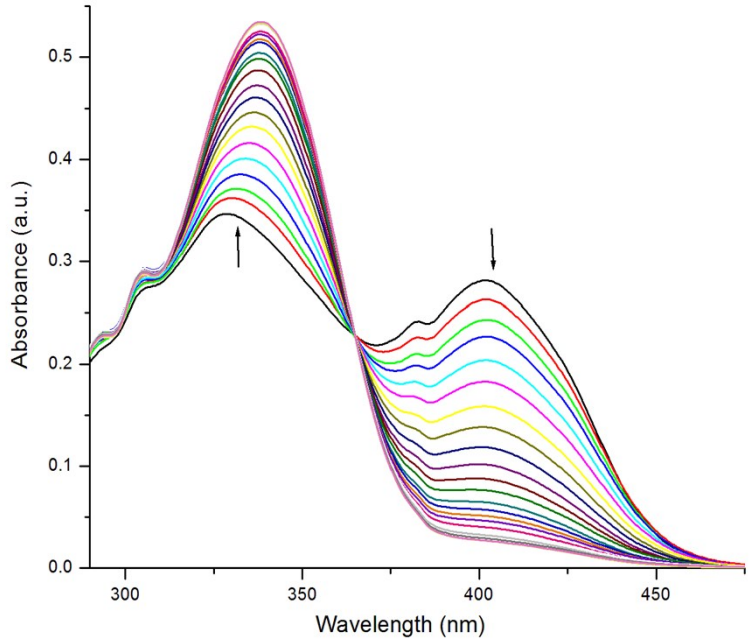

Fig. S27. Changes observed on incremental addition of HF_2^- (0.003 ml × 10^{-3} M each) to in situ formed **HVPh**-Mg^{2+} in DMSO (pH 7.2, HEPES buffer) in UV-vis spectra

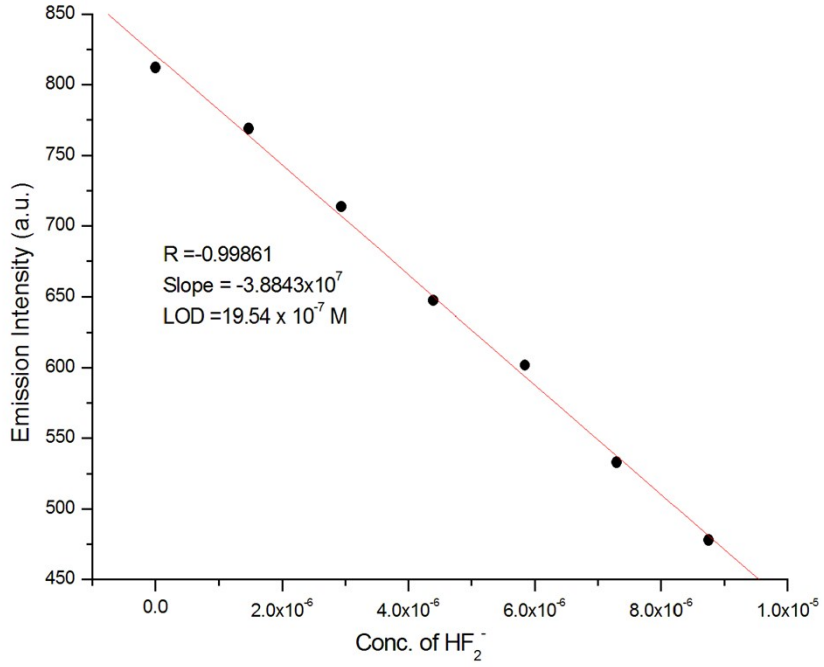

Fig S28 Calculation of limit of detection (LOD) for HF_2^-

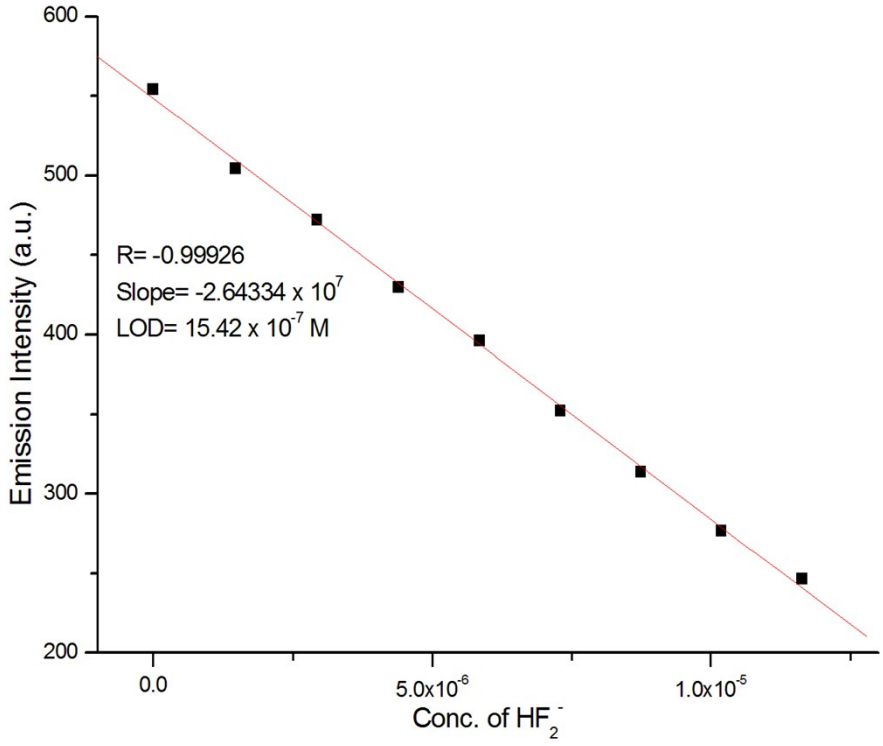

Fig S29 Calculation of limit of detection (LOD) for HF_2^-

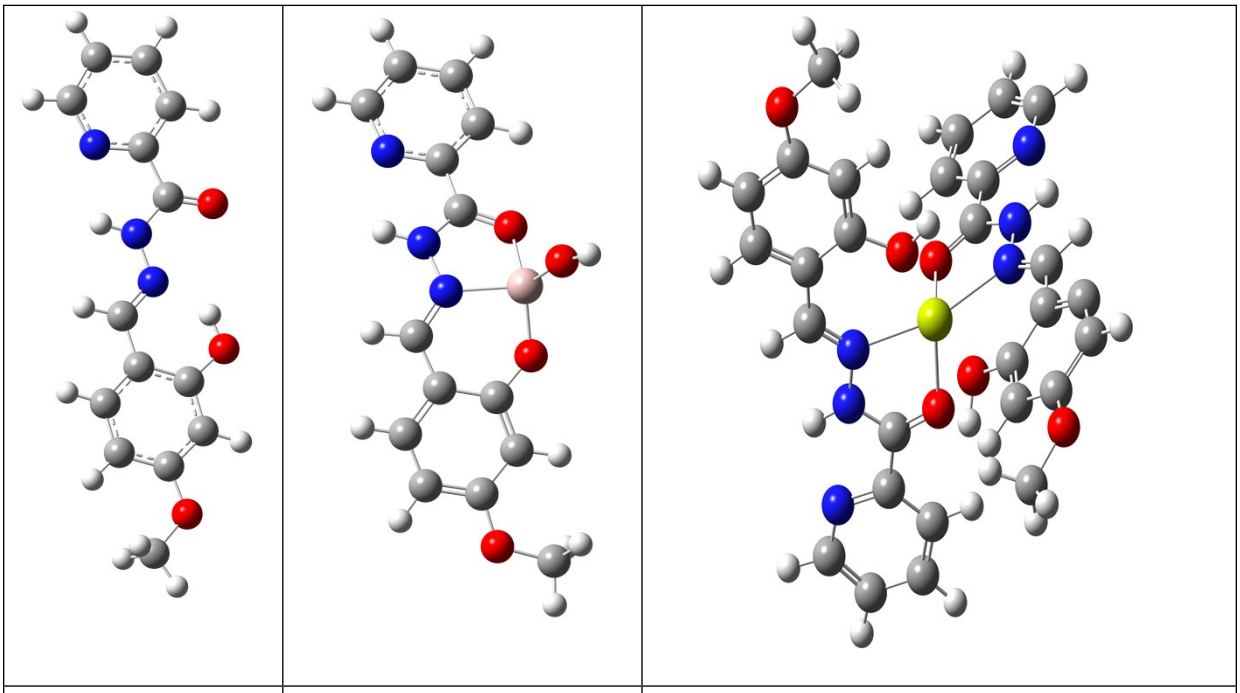

HVPh	**HVPh**-Al	**HVPh**-Mg

Fig 30 DFT/B3LYP optimised structure of **HVPh**, **HVPh**-Al and **HVPh**-Mg

Table S2 Contributions in MOs of **HVPh**

MOs	Energy (eV)	vanilin	picoyl hydrazide
LUMO+5	0.95	45	55
LUMO+4	0.9	7	93
LUMO+3	-0.04	99	1
LUMO+2	-1.1	34	66
LUMO+1	-1.46	17	83
LUMO	-2.16	17	83
HOMO	-5.81	68	32
HOMO-1	-6.33	98	2

HOMO-2	-7.23	1	99
HOMO-3	-7.44	56	44
HOMO-4	-7.74	26	74
HOMO-5	-7.92	3	97

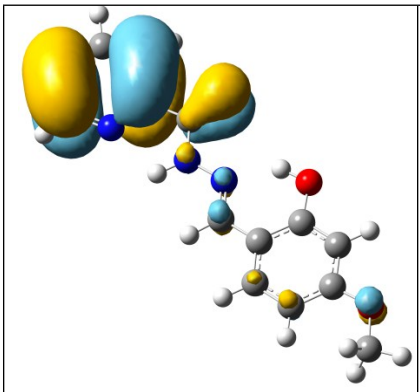	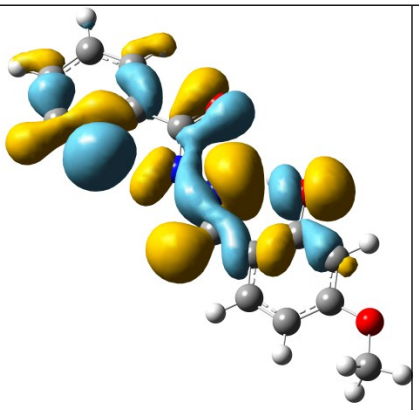	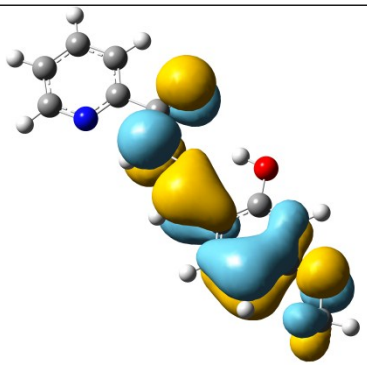
HOMO-5	HOMO-4	HOMO-3
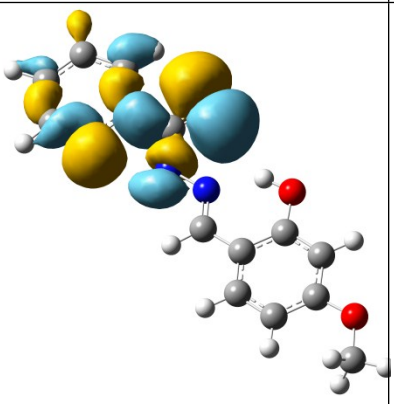	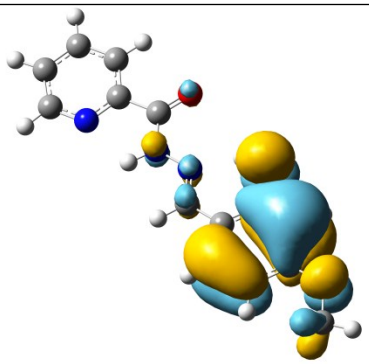	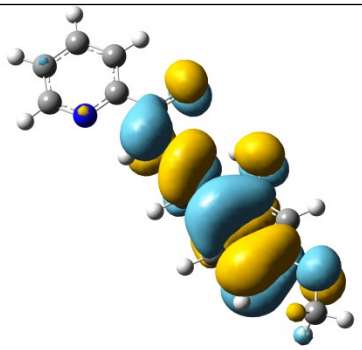
HOMO-2	HOMO-1	HOMO

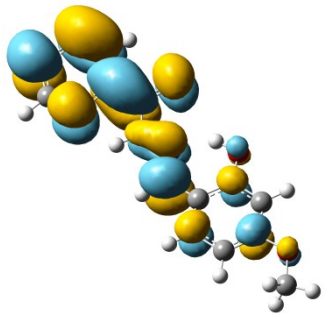	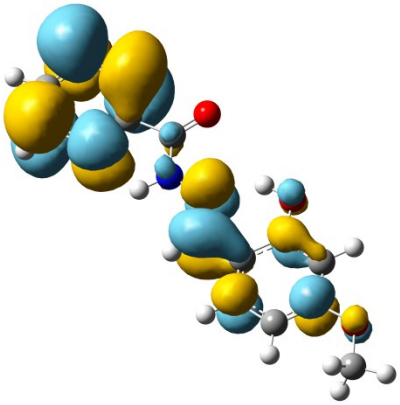	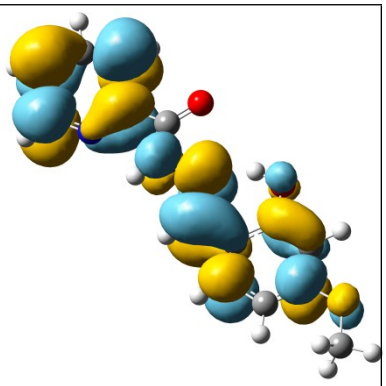
LUMO	LUMO+1	LUMO+2
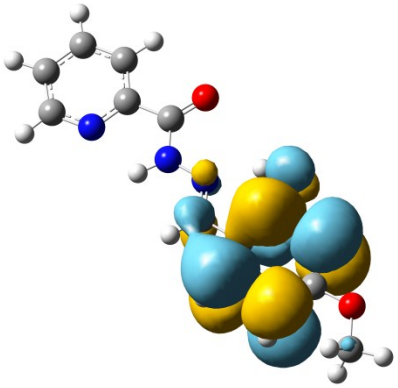	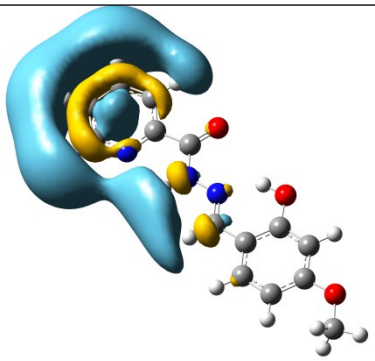	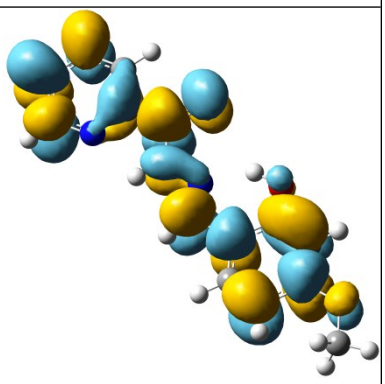
LUMO+3	LUMO+4	LUMO+5

Fig S31 Frontier molecular orbitals images of **HVPh**

Table S3 Contributions in MOs of **HVPh**-Al

MOs	Energy	vanilin	picoyl hydrazide	Al	OH
LUMO+5	-2.89	12	65	22	1
LUMO+4	-2.99	4	22	73	1
LUMO+3	-3.43	98	0	2	0
LUMO+2	-4.37	0	100	0	0
LUMO+1	-5.4	42	58	1	0
LUMO	-6.18	40	59	1	0

HOMO	-9.55	75	23	1	0
HOMO-1	-9.92	97	1	1	1
HOMO-2	-10.97	3	97	0	0
HOMO-3	-11.0	17	80	0	3
HOMO-4	-11.33	7	10	5	79
HOMO-5	-11.42	19	55	1	25

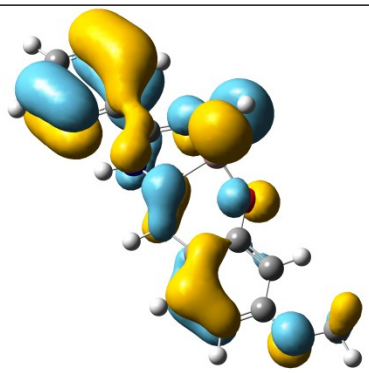	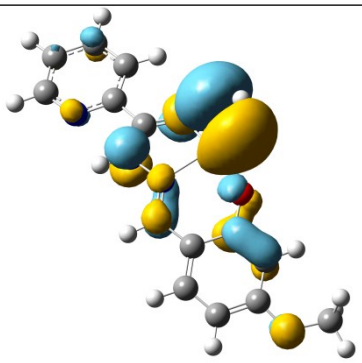	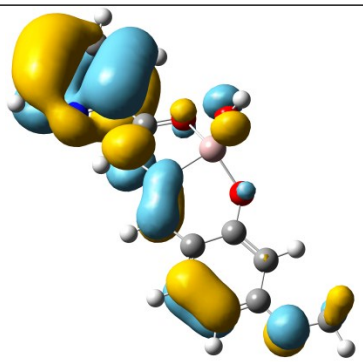
HOMO-5	HOMO-4	HOMO-3
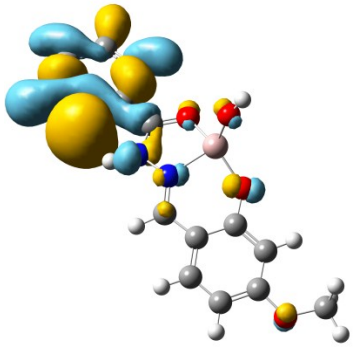	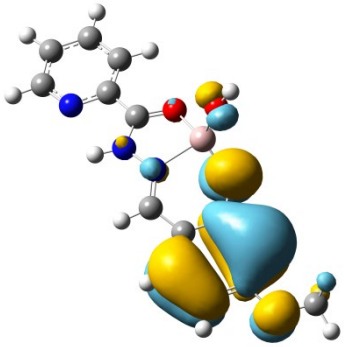	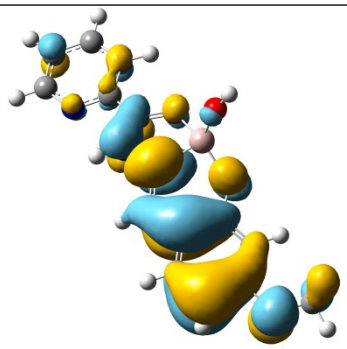
HOMO-2	HOMO-1	HOMO

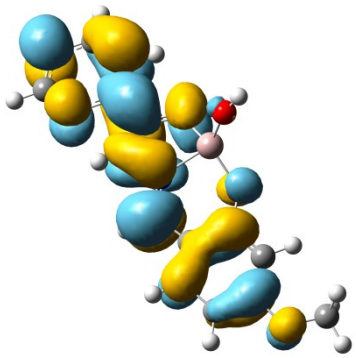	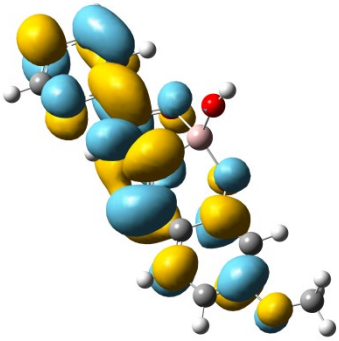	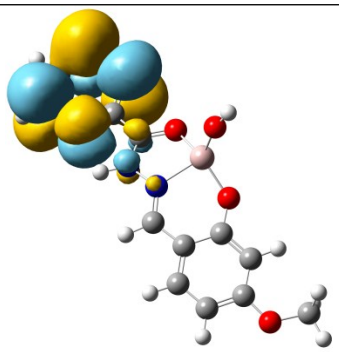
LUMO	LUMO+1	LUMO+2
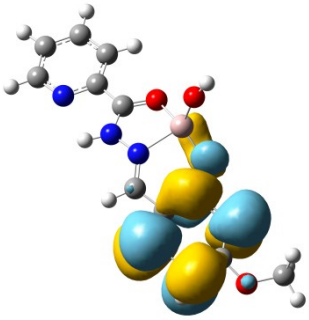	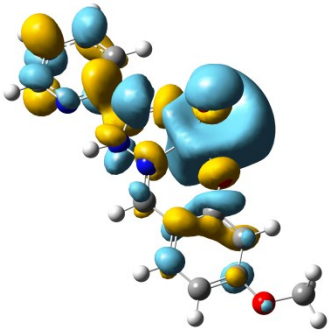	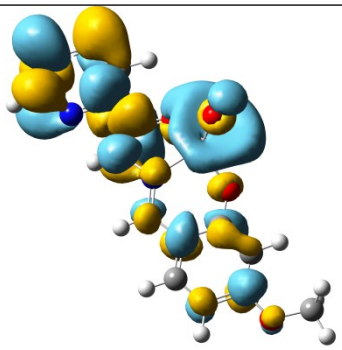
LUMO+3	LUMO+4	LUMO+5

Fig S32 Frontier molecular orbitals images of H**VPh**-Al

Table S4 Contributions in MOs of H**VPh**-Mg

MOs	Energy (eV)	picoyl hydrazide	vanilin	Mg
LUMO+5	-5.75	98	2	0
LUMO+4	-5.85	3	97	0

LUMO+3	-6.68	73	27	0
LUMO+2	-6.75	80	20	0
LUMO+1	-7.64	52	47	1
LUMO	-7.81	47	52	1
HOMO	-11.29	25	75	0
HOMO-1	-11.44	26	74	0
HOMO-2	-12.33	74	26	0
HOMO-3	-12.34	77	23	0
HOMO-4	-12.34	70	30	0
HOMO-5	-12.4	14	86	0

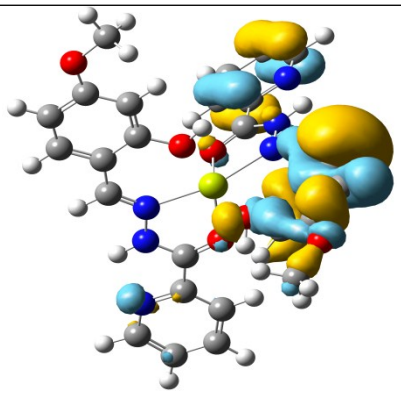	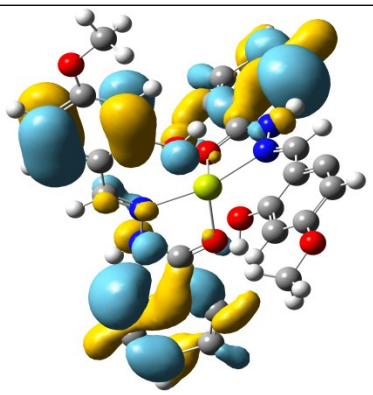	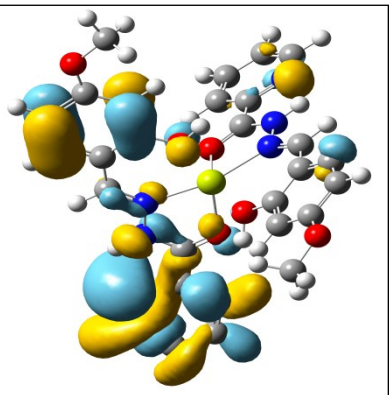
HOMO-5	HOMO-4	HOMO-3

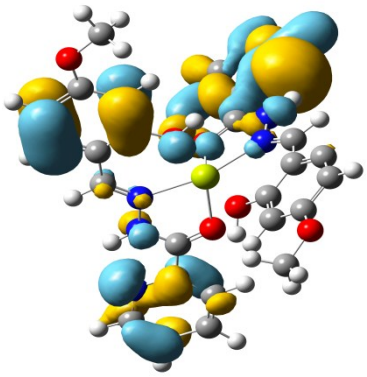	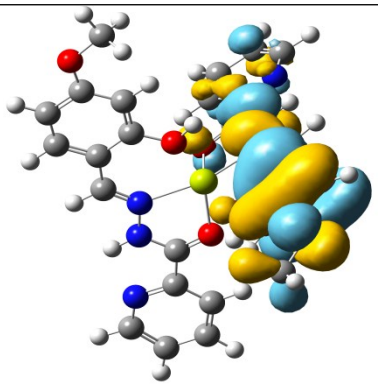	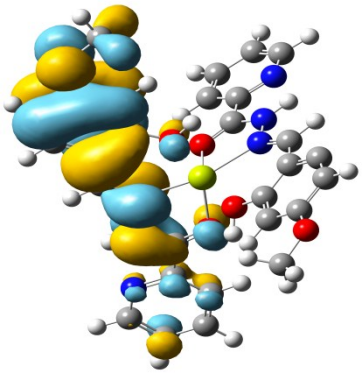
HOMO-2	HOMO-1	HOMO
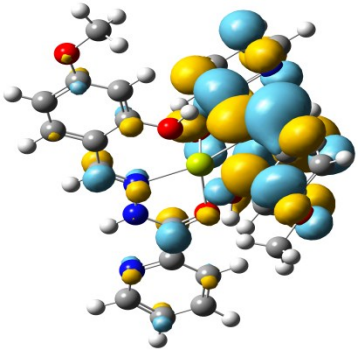	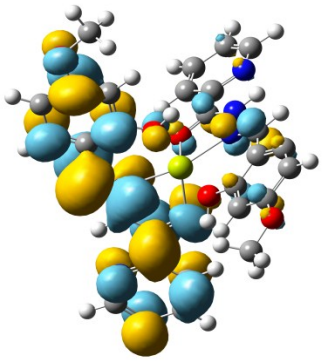	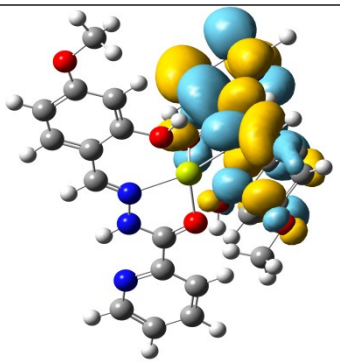
LUMO	LUMO+1	LUMO+2
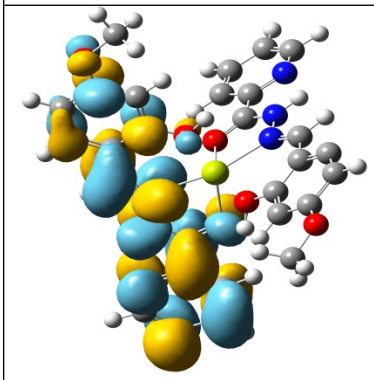	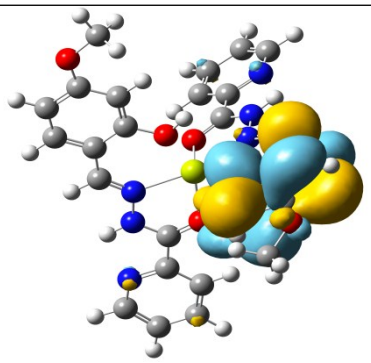	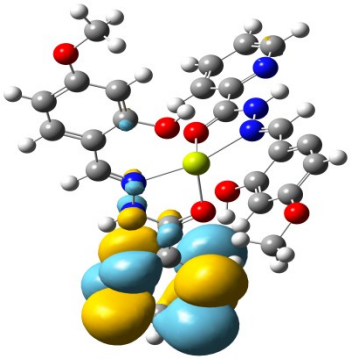
LUMO+3	LUMO+4	LUMO+5

Fig S33 Frontier molecular orbitals images of H**VPh**-Mg

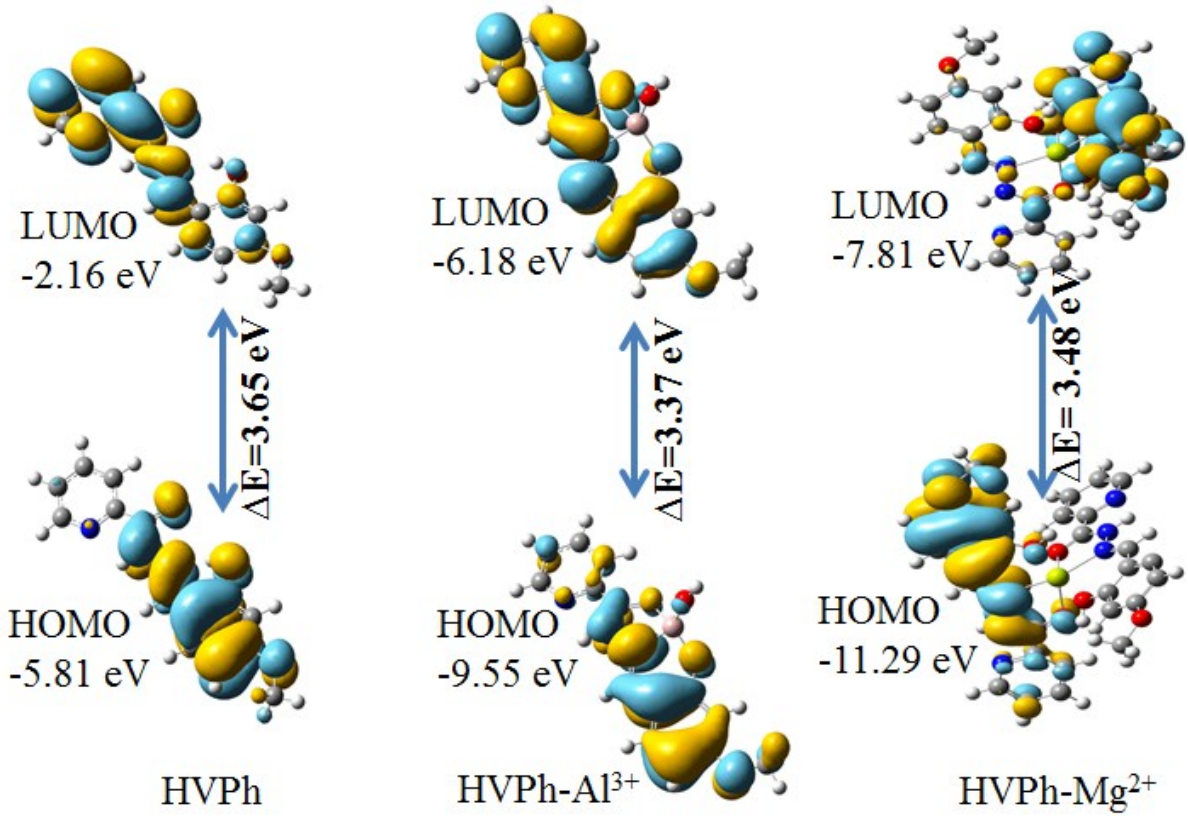

Fig 34 Frontier molecular orbitals that represent band gap (HOMO-LUMO gap) of **HVPh**, **HVPh**-Al and (**HVPh**)$_2$-Mg.

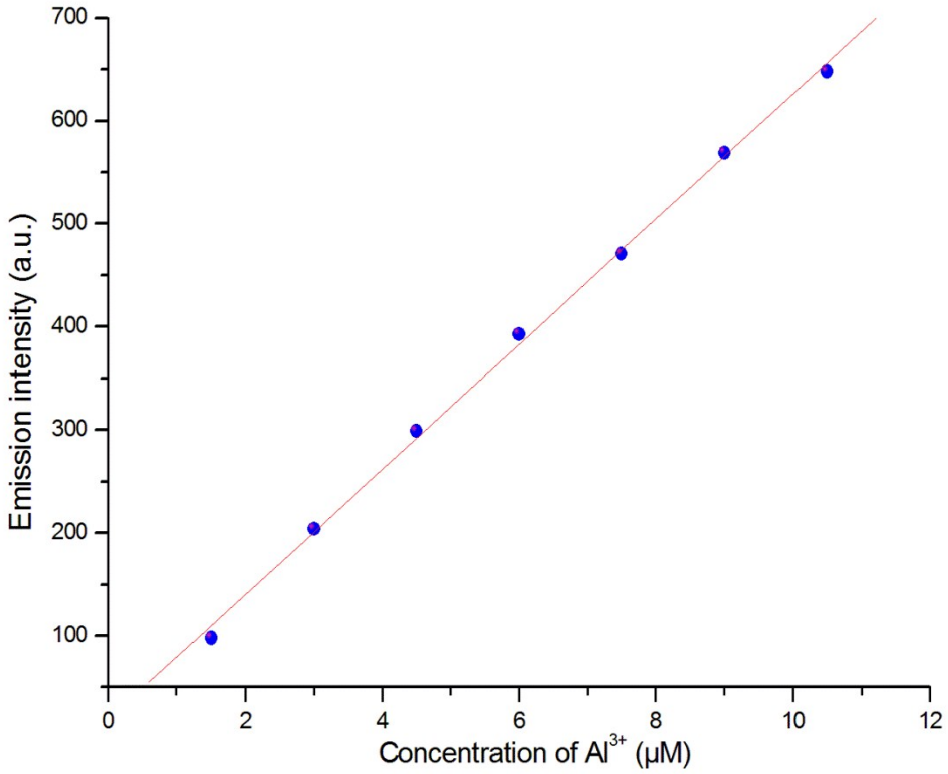

Fig S35 Calibration plot for detection of Al^{3+} using fluorescence active probe **HVPh**.